Robustness of STDP to spike timing jitter

Yihui Cui, Ilya Prokin, Alexandre Mendes, Hugues Berry, Laurent Venance

Robustness of STDP to spike timing jitter

Yihui CUI[1,#], Ilya PROKIN[2,3,#], Alexandre MENDES[1], Hugues BERRY[2,3,‡] and Laurent VENANCE[1, ‡,*]

[1]Dynamics and Pathophysiology of Neuronal Networks Team, Center for Interdisciplinary Research in Biology (CIRB), College de France, CNRS, INSERM, PSL Research University, Paris, France.

[2]INRIA, Villeurbanne, France

[3]University of Lyon, LIRIS UMR5205, Villeurbanne, France

[#]: co-first authors

[‡]: co-senior authors

[*]Correspondence: hugues.berry@inria.fr and laurent.venance@college-de-france.fr

ABSTRACT

In Hebbian plasticity, neural circuits adjust their synaptic weights depending on patterned firing. Spike-timing-dependent plasticity (STDP), a synaptic Hebbian learning rule, relies on the order and timing of the paired activities in pre- and postsynaptic neurons. Classically, in *ex vivo* experiments, STDP is assessed with deterministic (constant) spike timings and time intervals between successive pairings, thus exhibiting a regularity that differs from biological variability. Hence, STDP emergence from noisy inputs as occurring in *in vivo*-like firing remains unresolved. Here, we used noisy STDP pairings where the spike timing and/or interval between pairings were jittered. We explored with electrophysiology and mathematical modeling, the impact of jitter on three forms of STDP at corticostriatal synapses: NMDAR-LTP, endocannabinoid-LTD and endocannabinoid-LTP. We found that NMDAR-LTP was highly fragile to jitter, whereas endocannabinoid-plasticity appeared more resistant. When the frequency or number of pairings was increased, NMDAR-LTP became more robust and could be expressed despite strong jittering. Our results identify endocannabinoid-plasticity as a robust form of STDP, whereas the sensitivity to jitter of NMDAR-LTP varies with activity frequency. This provides new insights into the mechanisms at play during the different phases of learning and memory and the emergence of Hebbian plasticity in *in vivo*-like activity.

INTRODUCTION

Long-term changes in synaptic efficacy between neurons are thought to underlie learning and memory[1] and can be assessed with a synaptic Hebbian paradigm such as spike timing-dependent plasticity (STDP)[2–8]. In STDP, the occurrence of timing-dependent-long-term potentiation (tLTP) or -depression (tLTD) is the result of three factors. The two first ones are the two coincident activity patterns on either side of the synapse, which depends on 1) the relative timing between pre- and postsynaptic spikes (Δt_{STDP})[4,8], 2) the dendritic and axonal propagation delays[9], 3) the number of paired spikes ($N_{pairings}$)[10–13], 4) the frequency of the paired spikes ($F_{pairings}$)[6,7,10,11,14] and 5) membrane depolarization[14,15]; the third factor involves in STDP expression mainly refers to neuromodulators[16,17] and glial cells[18] .

STDP has been attracting a lot of interest in computational and experimental neurosciences because it relies on spike correlation and has emerged as a candidate mechanism for experience-dependent changes in neural circuits, including map plasticity[8,19–23]. STDP is classically investigated using regular repetitions of the same spike timing and fixed intervals between successive paired stimulations. A typical experimental protocol consists in pairing pre- and postsynaptic stimulations with a fixed Δt_{STDP} (ranging from -30 to +30ms for plasticity induction); $\Delta t_{STDP}<0$ when the postsynaptic stimulation occurs before the paired presynaptic one (post-pre pairings), whereas $\Delta t_{STDP}>0$ when the presynaptic stimulation occurs before the postsynaptic one (pre-post pairings). These pairings are then repeated between 15 and 200 times (between 0.1 and 5Hz) with the spike timing and the time interval between successive pairings being kept constant.

Regular stimulation paradigms produce patterns of activity that are likely to differ from the variability expected in *in vivo*-like firing. *In vivo* paired natural visual stimulations with postsynaptic action potential lead to Hebbian STDP with specific characteristics when compared to *ex vivo* STDP (broader membrane potential changes and STDP window), which

58 can be explained by jittered presynaptic inputs occurring *in vivo*[22]. A theoretical study has
59 started to explore naturalistic stimulations and showed that when neurons fire irregularly, the
60 impact of spike timing in plasticity becomes weaker than the influence of the firing rate[24].
61 However, whether STDP emergence and maintenance is robust against biological variability
62 remains to be investigated. To address this question, it is important to take into account
63 various forms of STDP, involving distinct intracellular signal transduction pathways, i.e.
64 NMDAR-, mGluR- or endocannabinoid(eCB)-mediated STDP[25–29] (for reviews see[8,30,31]). It
65 is thus expected that those various STDP forms might exhibit different robustness to spike
66 train variability.

67 Here, we show with patch-clamp recordings and mathematical modeling that corticostriatal
68 NMDAR- and eCB-STDP do not exhibit the same sensitivity to noisy spike timings: eCB-
69 plasticity (eCB-tLTD and eCB-tLTP) appeared robust to jittering whereas NMDAR-tLTP was
70 fragile. However, increasing the number or frequency of pairings improved NMDAR-tLTP
71 robustness. Our results further indicate that the robustness of NMDAR-tLTP to jitter is also
72 strengthened by the irregularity of the spike-train stimulations.

RESULTS

Corticostriatal synapses exhibit a bidirectional STDP in which NMDAR-tLTP, eCB-tLTD[29,32–34] or eCB-tLTP[12,13] are induced depending on the number of pairings (N_{pairings}) and the spike timing (Δt_{STDP}). While STDP is classically investigated using fixed Δt_{STDP}, we examine here the effect of noisy Δt_{STDP}, closer to *in vivo*-like firing. Here, we define the Inter-Pairing-Interval (IPI) as the time interval between two consecutive presynaptic stimulations, whereas Δt_{STDP} is the time interval between the post- and the presynaptic stimulation times within a given paired stimulation (in a "standard" STDP protocol both IPIs and Δt_{STDP} are constant).

NMDAR- and eCB-mediated STDP triggered with fixed Δt_{STDP}

We observed bidirectional asymmetric STDP in MSNs (Fig. 1a): 100 post-pre pairings (Δt_{STDP}<0) induced tLTP whereas 100 pre-post pairings (Δt_{STDP}>0) induced tLTD. An example of the tLTP induced by 100 post-pre pairings with fixed Δt_{STDP} (Fig. 1b) is illustrated in Figure 1c1. The input resistance Ri remained stable over this period. Although we fixed the values of Δt_{STDP}, they slightly vary from one pairing to another (Fig.1b). This low jitter can be written formally as $\Delta t_{\text{STDP}} = m_{\Delta t} + \xi_{\Delta t}$, were $m_{\Delta t}$ is the mean spike timing and $\xi_{\Delta t}$ is a random variable with mean 0 and standard deviation $\sigma_{\Delta t}$. Overall, 100 post-pre pairings induced tLTP (mean EPSC amplitude recorded 60 min after protocol induction: 149±13% of baseline, p=0.0028, n=13) (Fig. 1c2). $\sigma_{\Delta t}$ was 1.4±0.2ms (Fig. 1c3). This tLTP was NMDAR-mediated since prevented by D-AP5 (50 µM), a NMDAR antagonist, (88±12%, p=0.375, n=5; p<0.0001 when compared with tLTP in control) (Fig. 1c2). Conversely, pre-post pairings induced tLTD, as shown in the example in Figure 1d1. Overall, 100 pre-post pairings induced tLTD (76±7%, p=0.0070, n=10) (Fig. 1d2). $\sigma_{\Delta t}$ was 1.4±0.2ms (Fig. 1d3). This tLTD was

97 CB_1R-mediated since prevented by AM251 (3μM), a CB_1R specific inhibitor (99±2%,
98 p=0.816, n=5; p<0.0001 when compared with tLTD in control) (Fig. 1d2). We thus find an
99 anti-Hebbian polarity for corticostriatal STDP. We previously showed that GABA operates as
100 a Hebbian/anti-Hebbian switch at corticostriatal synapses[34,35] and corticostriatal STDP
101 polarity depends on the presence[32,33] or the absence[12,29,36,37] of $GABA_A$ receptor antagonists.

102 Besides this bidirectional STDP (NMDAR-tLTP and eCB-tLTD) induced for 100 pairings,
103 we reported that low numbers of pairings ($N_{pairings}$ =5-15) induce an eCB-tLTP, dependent on
104 the activation of CB_1R[12,13]. Figure 1e1 shows an example of tLTP induced by 10 post-pre
105 pairings. Overall, 10 post-pre STDP pairings induced tLTP (145±9%, p=0.0005, n=15), which
106 was prevented by AM251 (3μM) (76±10%, p=0.080, n=4; p<0.0001 when compared with
107 tLTP in control) (Fig. 1e2) as recently reported[12]. $\sigma_{\Delta t}$ for 10 post-pre parings STDP was
108 1.8±0.3ms (n=15) (Fig. 1e3). Note that there was no difference between the $\sigma_{\Delta t}$ measured for
109 NMDAR-tLTP, eCB-tLTD and eCB-tLTP (one way ANOVA, p=0.4094).

110

111 **A computer model emulates NMDAR- and eCB-mediated STDP**

112 To help interpret our experimental results, we used a mathematical model of the signaling
113 pathways implicated in corticostriatal STDP, including NMDAR- and CB_1R-plasticity[12,29,32,33]
114 (Fig. 1f1). The model is detailed in S1 Text, with parameter values listed in S1 and S2 Tables.
115 We include in the Supporting Information a thorough description of the mechanisms by which
116 eCB- and NDMAR-plasticity are expressed in the model when STDP protocol ($N_{pairings}$=100)
117 is applied (S3 Text). Figure 1f2 shows the value of the total synaptic weight (W_{total}) predicted
118 by the model with various $N_{pairings}$ and Δt_{STDP}. In agreement with the experimental data, with
119 small $\sigma_{\Delta t}$ (3ms), the model features three main plasticity regions: tLTD was observed for
120 short pre-post pairings (0<Δt_{STDP}<+30ms), whereas short post-pre pairings (-30<Δt_{STDP}<0ms)

induced a first tLTP region for low numbers of pairings (3<$N_{pairings}$<25) and a second tLTP region emerging for $N_{pairings}$>50. Blocking the NMDAR-CaMKII pathway in the model (Fig. 1f3) suppresses the second tLTP region whereas blocking CB_1R activation (Fig. 1f4) prevents the expression of tLTD and of the first tLTP region. Therefore, the model emulates both CB_1R-tLTD and -tLTP, in agreement with the eCB-tLTD and eCB-tLTP illustrated in the experimental data of Figure 1d and 1e, respectively. The model also faithfully emulates the appearance of NMDAR-tLTP for $N_{pairings}$>50.

Predicting the effects of jittered STDP with a mathematical model

The small jitter observed in the above experiments was the result of biological variability inherent to the experimental setup. Our next goal was to extend this study to larger jitters (3<$\sigma_{\Delta t}$<10ms) that we controlled experimentally. We first used constant intervals between two consecutive pairings (Inter-Pairing Interval, IPI) and used the same definition as above for jittered Δt_{STDP} (*Methods*): $\Delta t_{STDP} = m_{\Delta t} + \xi_{\Delta t}$, where $\xi_{\Delta t}$ is a random variable with zero mean and $m_{\Delta t}$ is the expected value of the spike timing Δt_{STDP} over the $N_{pairings}$. Next, we adjusted the probability distribution function and the variance of $\xi_{\Delta t}$ to perform a parametric exploration of the impact of jitter.

In Figure 2, the jitter $\xi_{\Delta t}$ was sampled from a uniform distribution in [-$\sigma_{\Delta t}$,+$\sigma_{\Delta t}$] (Fig. 2a1). STDP in the model was globally not robust to jitter, since the three forms of plasticity vanished when $\sigma_{\Delta t}$ was large enough (Fig. 2a2). However, the model delivered the prediction that the three forms of plasticity do not display the same sensitivity to jitter. In particular, NMDAR-tLTP is predicted to be very fragile when subjected to $\sigma_{\Delta t}$: its amplitude decreases as soon as $\sigma_{\Delta t}$>2ms and completely vanishes for $\sigma_{\Delta t}$>4ms (Fig. 2a2 and 2b2). In contrast,

eCB-plasticity is much less sensitive: eCB-tLTP is still present for jitters as large as 7-8ms and eCB-tLTD is still expressed with $\sigma_{\Delta t} = 10$ms (Fig. 2b3).

We next evaluated the validity of this prediction when the probability distribution function of the jitter changes. Figure 2 illustrates the results we obtained with Gaussian (Fig. 2c) or triangular (Fig. 2d) distributions of $\sigma_{\Delta t}$ (see *Methods*). In both cases, the profiles of the robustness curves (Fig. 2c2 and 2d2) are almost identical to each other and similar to the robustness curves obtained with a uniform distribution (Fig. 2a2). In Figure 2e, we combined a triangular distribution for $\sigma_{\Delta t}$ with random IPIs, i.e. in this case, stochasticity is applied not only to the timing between the two stimulations of a given pairing, but also to the time interval between two consecutive pairings: IPI distribution was Poisson with refractory period τ_r and rate λ (see *Methods*). Despite this increased stochasticity, we found that eCB-tLTD was again more robust, tolerating jitters up to 6-7ms (eCB-tLTP) or 10ms (eCB-tLTD) whereas NMDAR-tLTP was fragile, vanishing for $\sigma_{\Delta t}$>4ms (Fig. 2e2). Therefore, according to our model, the observation that eCB-STDP is more robust to jitter than NMDAR-tLTP could be a general property of the response of the signaling pathways to noisy paired stimulations.

Differential effect of jitter on NMDAR- and eCB-mediated plasticity

Based on the model predictions, we next investigated experimentally the sensitivity to jitter of NMDAR-tLTP induced by 100 post-pre pairings (Fig. 3a), using stochastic Δt_{STDP}, distributed according to Figure 2c1. As aforementioned, NMDAR-tLTP can be induced with a $\sigma_{\Delta t}$<3ms (Fig. 1c3). Increasing $\sigma_{\Delta t}$ beyond 3ms was sufficient to obliterate tLTP for 100 post-pre pairings. As exemplified (Fig. 3b and c1), 100 post-pre pairings with $\sigma_{\Delta t}$=7.9ms and centered on $m_{\Delta t}$ =-18ms failed to induce plasticity. Overall, we did not observe tLTP expression for

$\sigma_{\Delta t}$>3ms (92±2%, p=0.560, n=7; p<0.0001 when compared with tLTP observed without jitter) (Fig. 3c2 and c3) in agreement with the model prediction (Fig. 2c2).

We next investigated the robustness of the eCB-tLTD to the variability of Δt_{STDP}. We observed potent tLTD even with large values of $\sigma_{\Delta t}$. As shown in Figure 3d1, 100 pre-post pairings with $\sigma_{\Delta t}$=7.0ms centered on $m_{\Delta t=}$+18ms induced a large tLTD. Overall, we observed that tLTD was still induced for 100 pre-post pairings with 3<$\sigma_{\Delta t}$<10ms (70±6%, p<0.0001, n=14; p=0.1661 when compared with tLTD observed without jitter) (Fig. 3d2 and d3). The mean value of tLTD, observed for 3<$\sigma_{\Delta t}$<10ms, was not different from the one observed in control, i.e. for 0<$\sigma_{\Delta t}$<3ms (p=0.400).

Finally, we investigated the robustness of the eCB-tLTP to the variability of Δt_{STDP} and observed potent tLTP even with large values of jitter, i.e. up to $\sigma_{\Delta t}$~8ms. An example of tLTP induced by 10 post-pre pairings with $\sigma_{\Delta t}$=6.4ms centered on $m_{\Delta t}$=-21ms is illustrated in Figure 3e1. In summary, tLTP could be induced even for $\sigma_{\Delta t}$=8ms (160±12%, p=0.0021, n=9; p=0.0732 when compared with tLTP observed without jitter) (Fig. 3e2 and e3); the mean value of tLTP was not different from the one observed in control (p=0.1660).

We ensured that the $m_{\Delta t}$ absolute values were not different in control and jittered conditions for 100 post-pre pairings (18±2ms, n=13, *vs* 21±3ms, n=7, p=0.4711), 100 pre-post pairings (21±2ms, n=10, *vs* 21±2ms, n=14, p=0.8984), 10 post-pre pairings (17±2ms, n=15, *vs* 20±2ms, n=9, p=0.2297) or between these different STDP protocols (one-way ANOVA: p=0.4851) (Supplementary Fig. 1).

In conclusion, in agreement with our model prediction, whereas NMDAR-mediated tLTP appears fragile against the variability of Δt_{STDP}, eCB-plasticity (eCB-tLTD as well as eCB-tLTP) exhibits a large robustness for the temporal imprecision of Δt_{STDP}.

191

192 **Model-based analysis of the effects of jittering**

193 The above experimental results provide us with a validation of our mathematical model. We
194 next used this validated model as a tool to investigate the molecular mechanisms behind these
195 differences of robustness.

196 We have shown in a previous study that eCB-tLTP was expressed when the amount of eCBs
197 produced was large enough that the fraction of activated CB_1R, y_{CB1R}, overcomes a threshold
198 θ_{LTP}^{start} [13]. In the absence of added noise, $\sigma_{\Delta t} = 0$, our experimental data shows that as few as 5
199 pairings at 1Hz and Δt_{STDP}=-15ms are enough to trigger eCB-tLTP[12]. Accordingly, our model
200 produces large amounts of eCBs in the first 5-10 pre-post pairings so that y_{CB1R} reaches θ_{LTP}^{start}
201 after as few as 5 pairings (Fig. 4a1). When $\sigma_{\Delta t}$ =5ms jitter was added to $m_{\Delta t} = -15$ms,
202 some of the pairings failed to deliver y_{CB1R} transients of maximal amplitude (Fig. 4a2). But
203 for $\sigma_{\Delta t}$<7-8ms, a number of y_{CB1R} transients still had sufficient amplitude to overcome θ_{LTP}^{start},
204 which was enough to trigger eCB-tLTP (Fig. 4a2). When $\sigma_{\Delta t}$ was large though (e.g. 10ms),
205 the y_{CB1R} transients failed to reach the LTP zone and eCB-tLTP was not expressed (Fig. 4a3).

206 In experiments without added jitter, eCB-tLTD progressively accumulates when $N_{pairings}$
207 increases and starts to be significant for $N_{pairings}$>25[12]. In the model with $m_{\Delta t} = +20$ms and
208 $\sigma_{\Delta t}$ =0, the y_{CB1R} transients remain in the LTD area for the most part of the STDP pairings
209 (Fig. 4a3). To account for the progressive accumulation of eCB-tLTP with $N_{pairings}$, each
210 transient in the model contributes a small decrease of the synaptic weight. Even with large
211 amounts of jitter (see e.g. $\sigma_{\Delta t}$ =5 or 10ms in Figure 4a2-a3) y_{CB1R} transients remain mostly
212 inside LTD area so eCB-tLTD remains expressed even with large jitter.

213

The robustness of NMDAR-tLTP is predicted to be frequency-dependent

Experimentally, NMDAR-tLTP ($m_{\Delta t} = -15$ms and $\sigma_{\Delta t} = 0$) was observed at F_{pairings}=1Hz when N_{pairings}>50, beyond which its amplitude did not depend much on N_{pairings}[13]. To account for this feature, the steady-state concentration of activated CaMKII, that sets W_{post} in the model, is bistable: 45 min after the stimulation, CaMKII was either almost fully inactivated ("no plasticity" state) or almost fully activated ("LTP" state)[13,38]. When the frequency of post-pre pairings (-30<Δt_{STDP}<0ms) was large enough (i.e. F_{pairings}≥1Hz), the IPI was smaller than the decay time of the CaMKII activation transient triggered by each post-pre pairings (Fig. 4b1). As a result, in the absence of added noise ($\sigma_{\Delta t} = 0$), the CaMKII activation transients progressively built up on top of each other. The accumulated CaMKII activation overcomes the threshold between the "no plasticity" and the "LTP" states only for N_{pairings}>50 (Fig. 4b1)[13]. With jitter (e.g. $\sigma_{\Delta t} = 5$ms in Fig. 4b2 or 10ms in Fig. 4b3), many of the IPIs were either too long or too short to trigger maximal amplitude transients of activated CaMKII. As a result, CaMKII activation never reached the threshold, thus explaining the fragility of NMDAR-tLTP with respect to jittering (at 1Hz).

A major indication from the above analysis is the importance of the IPI frequency for the robustness of NMDAR-tLTP to jitter. Figure 5 compares the robustness to jitter for constant IPI with F_{pairings}=1Hz (Fig. 5a) and 1.05Hz (Fig. 5b). The size of the green area that locates eCB-tLTD on Figure 5a2-b2 was not much altered by the increase of the pairing frequency. Likewise, the size of the red area that locates eCB-tLTP in Figure 5a1-b1 did not vary much when the frequency was increased. However, the size of the red area locating NMDAR-tLTP increased drastically with frequency (Fig. 5a2-b2). Therefore, our model predicts that NMDAR-tLTP should become more robust to jitter at larger frequencies, whereas eCB-tLTP and eCB-tLTD are not significantly changed.

Several aspects of glutamate signaling at the corticostriatal synapse are known to display complex frequency-dependence[39]. Our model is calibrated with experimental data at 1Hz and features none of the above frequency dependencies. Therefore, we cannot expect a precise quantitative match between experiments and model when frequency is varied below or above 1Hz. However, the model still yields correct predictions of the main qualitative trends observed in the experiments, since the effects of a small change of F_{pairings} in the model (1.00 to 1.05Hz) were similar to the effects of larger changes (1 to 3Hz) in the experiments[13]. Therefore, in the experiments, we expect to observe a change of robustness pattern similar to Figure 5b, around F_{pairings}=3Hz rather than 1.05Hz.

Increasing F_{pairings} and N_{pairings} stabilized NMDAR-tLTP against jitter

We next tested experimentally whether an increase from 1 to 3Hz of STDP pairings would protect the NMDAR-tLTP against jitter, as predicted by the model. As shown in Figure 6a1, 100 post-pre pairings at 3Hz with $\sigma_{\Delta t}$=9ms and centered on $m_{\Delta t}$ =-22ms induced tLTP. Overall, we observed tLTP for 100 post-pre pairings applied at 3Hz with 4<$\sigma_{\Delta t}$<9ms (181±30%, p=0.0274, n=9) (Fig. 6a2 and a3); the mean value of these tLTP observed at 3Hz with 4<$\sigma_{\Delta t}$<9ms were not significantly different from the one observed with stimulation-related $\sigma_{\Delta t}$<3ms at 1Hz (p=0.520). When we plotted the magnitude of plasticity against $\sigma_{\Delta t}$ for 100 post-pre pairings at 3Hz, we observed that tLTP was still induced even for $\sigma_{\Delta t}$=9ms (Fig. 6a3). We observed different synaptic efficacy changes following 100 post-pre pairings at 1Hz with and without jitter and at 3Hz with jitter (ANOVA, p<0.0001). The NMDAR-tLTP thus acquires certain robustness to the variability of Δt_{STDP} with increasing frequency of pairings.

We next investigated whether a higher N_{pairings} would secure the expression of NMDAR-tLTP even with $\sigma_{\Delta t}$>3ms (Fig. 6b). When we doubled N_{pairings} we did not observe expression of significant tLTP. Indeed, 200 post-pre pairings (-30<$m_{\Delta t}$<0ms with 3<$\sigma_{\Delta t}$<10ms) did not induce plasticity (112±9%, p=0.236, n=6; Fig. 6b3) but when we increased N_{pairings} up to 250-300, tLTP was reliably observed with $\sigma_{\Delta t}$>3ms. Figure 6b1 shows an example of tLTP induced by 250 pairings with $\sigma_{\Delta t}$=5ms and centered on -20ms. Overall, 250-300 post-pre STDP pairings (-30<$m_{\Delta t}$<0ms with 3<$\sigma_{\Delta t}$<10ms) induced tLTP (170±10%, p=0.0012, n=6; Fig. 6b2 and b3); the mean values of these tLTP observed for N_{pairings}=250-300 at 1Hz with 4<$\sigma_{\Delta t}$<9ms were not different compared to tLTP induced with 100 post-pre pairings at 1Hz with $\sigma_{\Delta t}$<3ms (p=0.1952). We observed different synaptic efficacy changes following 100, 200 and 250-300 post-pre pairings (ANOVA, p<0.0001).

Transitions from spike-timing- to frequency-dependent plasticity

We next tested with our mathematical model whether the robustness of STDP to jitter of the spike timing depends on the regularity of the spike train. In Figure 2e, we show an example of the combination of stochastic spike timings (triangular distribution) with stochastic IPIs (Poisson distributed) with a constant and relatively large refractory period τ_r (see *Methods-Mathematical model, Protocol 4*). However, when τ_r decreases, short IPIs are more frequently sampled and the train of presynaptic stimulation becomes more irregular. Therefore, through variations of the refractory period τ_r, the presynaptic stimulation can be progressively switched from highly irregular to regular spike trains.

Figure 7 shows model predictions for the alteration of the robustness curves when τ_r varies. With high refractory period, *i.e.* when $\tau_r \approx F_{\text{pairings}}$, the IPIs are weakly noisy, so one recovers the robustness curves of Figure 2e, with eCB-STDP being more robust than

NMDAR-tLTP. However, when τ_r is 70% of F_{pairings}, the robustness of both eCB-tLTP and NMDAR-tLTP increases and both exhibit similar robustness. With even smaller values of τ_r, NMDAR-tLTP becomes more robust than eCB-tLTP. Moreover, eCB-tLTD (F_{pairings}=1Hz, $m_{\Delta t} = +20$ms, N_{pairings}=100) progressively stops triggering LTD when τ_r decreases, even inducing LTP for very low τ_r. Hence, when the presynaptic spike train is progressively switched from regular to very irregular spike trains, two main changes occur: (*i*) the three plasticity forms (NMDAR-tLTP, eCB-tLTD and eCB-tLTP) become increasingly robust to jittering (at the limit of highly irregular spike trains, jittering hardly affects plasticity amplitudes), and (*ii*) eCB-tLTD is progressively changed to LTP, so that highly irregular paired stimulations with F_{pairings}=1Hz only produce LTP regardless of the sign of the spike timing.

DISCUSSION

Here, we have introduced jittered STDP protocols as noisy variants of STDP protocols where the spike timing, *i.e.* the delay between a presynaptic and paired postsynaptic stimulation (or vice-versa), is a random variable. Our results show that the magnitude of variability that STDP can tolerate varies depending on the pairing frequency and on the STDP form, i.e. NMDAR-tLTP, eCB-tLTP or eCB-tLTD. At 1Hz pairing frequency, eCB-STDP (eCB-tLTD and eCB-tLTP) is much more robust than NMDAR-dependent tLTP. However, this robustness depends on the number and frequency of pairings. Indeed, increasing the average pairing frequency to 3Hz improved the robustness of NMDAR-tLTP. We observed a similar improvement of the robustness of NMDAR-tLTP to jitter when the number of pairings increased more than two folds.

These results have wide-ranging implications for STDP expression in *in vivo*-like firing. They indicate that eCB-STDP could be more likely responsible for fast learning involving few trials (eCB-tLTP) or for learning at lower activity frequency than NMDAR-STDP. NMDAR-STDP could however take part in learning for larger frequencies or when the same spike timing recurs a large number of times during sustained activity. It also implies that in synapses where NMDAR is the main coincidence detector for tLTD or tLTP[3,5,6,40–42], a high degree of precision of the spike timing, and/or an increased number or frequency of pairings, are required for the emergence of the NMDAR-mediated plasticity. This can be viewed as a mechanism preventing the occurrence of spurious plasticity for noisy neural network activity. At synapses in which NMDAR and endocannabinoids are both involved in STDP expression[12,13,25–27,33,43] and in which eCB-LTP can occur, as it is the case in the striatum[12,13], the hippocampus[44–48] or the neocortex[49] the emergence of STDP would be possible even in noisy conditions and could thus serve subsequently as a priming for the subsequent expression of NMDAR-tLTP.

In the present study, we explored the robustness of STDP when noise affects not only the spike timing but also the inter-pairing interval (IPI), i.e. the delay between two successive pairings. In the absence of jitter of the spike timing, our model predicts that IPI irregularity tends to consolidate tLTP at the expense of tLTD. This prediction that irregular IPIs strengthen tLTP when the spike timing is constant confirms the result obtained independently and with different mathematical models[7,19,22,24]. When IPIs are regular, adding jitter of the spike timing in our model progressively suppresses STDP. However, with more irregular IPIs our model predicts that the three STDP forms should exhibit larger robustness to noise. Therefore our result suggests that jittering of the spike timing has larger impact on STDP when the IPIs are regular, but that jittering has much less consequence with irregular IPIs. Experimental testing of this model prediction would greatly improve our understanding of the induction and maintenance of STDP in *in vivo*-like firing.

Subthreshold postsynaptic depolarization is a key factor in the induction of plasticity[50]. The existence of plasticity induced by STDP-like protocols without postsynaptic spikes (subthreshold-depolarization-dependent plasticity, SDDP) has been reported in the neocortex[51], striatum[52] and hippocampus[53]. In the striatum, SDDP differs from STDP on two aspects: (*i*) SDDP was induced in a larger temporal window ($-100<\Delta t_{STDP}<+100$ms) and (*ii*) tLTP and tLTD were induced regardless of the spike timing. Therefore, the action potential would not be necessary for plasticity induction, but determinant for the STDP polarity and the width of the Δt_{STDP}. The effects of jitter remain to be determined on SDDP, *i.e.* subthreshold events.

The polarity of plasticity depends greatly on the frequency of stimulus presentation. Indeed, prolonged firing activity at low and high frequency promote LTD and LTP, respectively, at the same synapses in hippocampus[54–56]. However, alteration of a regular low-frequency stimulation (900 stimulations at 1Hz) with Poisson-distributed interstimulus intervals (as an

approximation of naturalistic patterns) prevents LTD expression in the neocortex[57]. Interestingly, this LTD induced with regular low-frequency stimulation has been reported to be NMDAR-mediated[58], and we show here that NMDAR-plasticity is fragile to jitter especially for low firing rate (1Hz). It remains thus to investigate in a rate-based paradigm whether Poisson stimulation would erase LTD induced by higher firing rate (3-5Hz[54]). Various forms of naturalistic patterns as an attempt to mimic *in vivo* activity have been experimentally tested for plasticity expression: from single burst of dendritic spikes, which induced NMDAR-LTP in hippocampus[59] and NMDAR-LTD in neocortex[60], to noisy STDP-like protocols[7,19,20,22] and burst-timing-dependent plasticity paradigms[61]. Based on data harvested in the neocortex, a phenomenological computer modeling showed that for constant frequencies but random spiking, LTP wins over LTD with increasing frequency[7]. Activity patterns recorded *in vivo* during specific behavioral tasks have been replayed *ex vivo* to test their ability to induce plasticity[19,56,62]. When sequences of spike trains recorded *in vivo* from visual cortex of the anaesthetized cat in response to natural scenes were replayed *ex vivo* in layer 2/3 pyramidal cells of rat visual cortex, both LTP and LTD was observed experimentally and modeling suggested the importance of suppressive interactions between spikes[19]. In the dentate gyrus, *in vivo* patterns recorded in granule cell during a task of delayed nonmatch-to-sample were able in most of the cases to induce LTP at mossy fibers[56]. Similarly, when hippocampal place cells activity recorded *in vivo* were replayed *ex vivo*, NMDAR-LTP (also dependent on cholinergic tone) was observed[62]. Natural stimuli recruit various neuronal circuits leading to presynaptic jitter, which can have important physiological consequences. Indeed, *in vivo* visually driven presynaptic inputs induce presynaptic jitter leading to broader membrane potential events, and can consequently promote a spatial reorganization of the responses of neurons to neighboring stimuli within a receptive field, as demonstrated in the rat visual cortex[22].

The debate about the nature of the neural coding, i.e. rate versus time codes[63–65], is prominent when studying STDP. It remains to be tested with mathematical models and experiments whether activity patterns of various vigilance states differently result in the emergence of spike- or rate-coding plasticity. At most of the synapses both rate and time codes co-exist; for example at CA1 synapses, stimuli induced LTD at 2-3Hz, no plasticity at 10Hz and LTP at 50 Hz demonstrating a rate code[54], and time codes are also supported as illustrated by the expression of various forms of STDP at the same synapse[11]. An answer to this debate could be that both rate and time codes work together for plasticity expression, as recently shown in the somatosensory cortex[66], but their relative contribution *in vivo* would depend on the ongoing activity (low or high), the cerebral structures, the noise level, the neuromodulatory systems at play and the signaling pathways involved in plasticity expression (as shown in the present study). Briefly, it appears that STDP can emerge form low frequency activity whereas rate codes would take over for higher frequency ranges[7,19,20,22].

A major conclusion from our present work is that the robustness of STDP to jitter depends on the underlying signaling pathways. For instance, the robustness of NMDAR-tLTP in our model is dependent on the amplitude of the activated CaMKII transients triggered by each post-pre pairings or on alterations of the ratio between the decay time of these transients and the IPIs. The robustness of STDP to jitter could be similarly controlled by quantitative variations in the underlying pathways. Such variations are expected to occur between two neuronal subtypes or brain regions but also as a result of the activation of a neuromodulatory pathway. Therefore, our work suggests that the expression of STDP in *in vivo*-like firing might appear or disappear as a result of modulations of its robustness to jitter, depending on the properties of the incoming patterns (reflecting for example fast learning or heavy training), but also on the brain region and, more transiently, on the activation of neuromodulatory pathways.

METHODS

Animals and brain slice preparation

OFA (Oncins France Strain A) rats (Charles River, L'Arbresle, France) were used at postnatal day 25-32 for brain slice electrophysiology. All experiments were performed in accordance with the guidelines of the local animal welfare committee (Center for Interdisciplinary Research in Biology Ethics Committee) and the EU (directive 2010/63/EU). The experimental protocol (ref. 2017-02 N° 2016120110255176) was approved by the Ethics Committee in Charge of Animal Experimentation (Paris Centre et Sud). Every precaution was taken to minimize stress and the number of animals used in each series of experiments. Animals were housed in standard 12 hours light/dark cycles and food and water were available *ad libitum*. Horizontal brain slices containing the somatosensory cortical area and the corresponding corticostriatal projection field were prepared as previously described[36]. Corticostriatal connections (between somatosensory cortex layer 5 and the dorso-lateral striatum) are preserved in the horizontal plane. Brain slices (330µm-thick) were prepared with a vibrating blade microtome (VT1200S, Leica Microsystems, Nussloch, Germany). Brains were sliced in an ice-cold cutting solution (125mM NaCl, 2.5mM KCl, 25mM glucose 25mM $NaHCO_3$, 1.25mM NaH_2PO_4, 2mM $CaCl_2$, 1mM $MgCl_2$, 1mM pyruvic acid) through which 95% O_2/5% CO_2 was bubbled. The slices were transferred to the same solution at 34°C for one hour and then to room temperature.

Patch-clamp recordings

Patch-clamp recordings were performed as previously described[12,18]. Briefly, for whole-cell recordings in borosilicate glass pipettes of 5-7 MΩ resistance were filled with (in mM): 122 K-gluconate, 13 KCl, 10 HEPES, 10 phosphocreatine, 4 Mg-ATP, 0.3 Na-GTP, 0.3 EGTA

(adjusted to pH 7.35 with KOH). The composition of the extracellular solution was (mM): 125 NaCl, 2.5 KCl, 25 glucose, 25 $NaHCO_3$, 1.25 NaH_2PO_4, 2 $CaCl_2$, 1 $MgCl_2$, 10 µM pyruvic acid bubbled with 95% O_2 and 5% CO_2. Signals were amplified using EPC10-2 amplifiers (HEKA Elektronik, Lambrecht, Germany). All recordings were performed at 34°C (Bath-controller V, Luigs&Neumann, Ratingen, Germany) and slices were continuously superfused with extracellular solution, at a rate of 2 ml/min. Slices were visualized under microscope (BX51WI Olympus, Rungis, France), with a 4x/0.13 objective for the placement of the stimulating electrode and a 40x/0.80 water-immersion objective for the localization of cells for whole-cell recordings. Current- and voltage-clamp recordings were filtered at 5 kHz and sampled at 10 kHz, with the Patchmaster v2x32 program (HEKA Elektronik).

Spike timing-dependent plasticity protocols: regular and jittered patterns

Electrical stimulations were performed with a concentric bipolar electrode (Phymep, Paris, France) placed in layer 5 of the somatosensory cortex. Electrical stimulation was monophasic, at constant current (ISO-Flex stimulator, AMPI, Jerusalem, Israel). Cortical stimulations evoked glutamatergic excitatory postsynaptic currents (EPSCs) (inhibited by CNQX 10µM and D-AP5 50µM, n=6) and not significantly affected by GABAergic events; Indeed, blocking $GABA_A$Rs with picrotoxin (50µM) did not significantly affect EPSC amplitude at corticostriatal synapses (123±31pA before and 118±26pA after picrotoxin, p=0.500, n=5). MSNs were kept at their resting membrane potential (-74.6±0.6 mV, n=90) and repetitive control stimuli were applied at 0.1Hz. Currents were adjusted to evoke 50-200 pA EPSCs. STDP protocols consisted of pairings of pre- and postsynaptic stimulations (at 1Hz) separated by a specific time interval (Δt_{STDP}). The paired stimulations were applied at 1Hz throughout the study except in Figure 6a1 and 6a2 in which 3Hz stimulations were tested. Presynaptic stimulations corresponded to cortical stimulations and the postsynaptic stimulation of an

445 action potential evoked by a depolarizing current step (30ms duration) in MSNs. Δt_{STDP}<0ms
446 for post-before-pre pairings, and Δt_{STDP}>0ms for pre-before-post pairings. Neuronal
447 recordings on neurons were made over a period of 10 minutes at baseline, and for at least 60
448 minutes after the STDP protocols. EPSC baseline stability was assessed by comparing the
449 average of the EPSC magnitude of the two first and the two last minutes of baseline; if the
450 variation of amplitude exceeded 10%, the experiment was discarded[4]. Recordings were
451 stopped if the injected current was larger than 50 or 100-150 pA during the baseline and after
452 pairings, respectively. We individually measured and averaged the amplitude of 60 successive
453 EPSCs from both baseline and 45-55 minutes after STDP protocol, in which the latter was
454 normalized by the former to calculate long-term synaptic efficacy changes. Neuron recordings
455 were made in voltage-clamp mode during baseline and for the 60 minutes of recording after
456 the STDP protocol, and in current-clamp mode during STDP protocol. Experiments were
457 excluded if the input resistance (Ri), measured every 10 sec all along the experiment, varied
458 by more than 20% during the very same time period where the EPSC amplitude were
459 measured for plasticity assessment: 10 minutes of baseline and the 10 last minutes of the
460 recording (generally 45-55 minutes after pairings). After recording of 10 min control baseline,
461 drugs were applied in the bath. A new baseline with drugs was recorded after a time lapse of
462 10 min (to allow the drug to be fully perfused) for 10 min before the STDP protocol. Drugs
463 were present until the end of the recording. All chemicals were purchased from Tocris
464 (Ellisville, MO, USA), except for picrotoxin (Sigma). DL-2-amino-5-phosphono-pentanoic
465 acid (D-AP5; 50µM) and 6-cyano-7-nitroquinoxaline-2,3-dione (CNQX; 10µM) were
466 dissolved directly in the extracellular solution and bath applied. N-(piperidin-1-yl)-5-(4-
467 iodophenyl)-1-(2,4-dichlorophenyl)-4-methyl-1H-pyrazole-3-carboxamide (AM251; 3µM)
468 and picrotoxin (50µM) were dissolved in ethanol and added to the external solution, such that
469 the final concentration of ethanol was 0.01-0.1%.

For the jittered Δt_{STDP} patterns, we used the following algorithm (see Protocol 2, below). We note t_{pre_i} and t_{post_i} the times of the presynaptic and postsynaptic stimulations in the paired stimulation number *i,* respectively. To set them, we first fixed the times of each presynaptic stimulation using the pairing frequency, i.e. $t_{\mathrm{pre}_i} = \frac{i}{F_{\mathrm{pairings}}}$. The postsynaptic times were then chosen randomly according to $t_{\mathrm{post}_i} = t_{\mathrm{pre}_i} + m_{\Delta t} + \xi_{\Delta t,i}$ where $m_{\Delta t}$ is the average spike timing and $\xi_{\Delta t}$ is a random variable with mean 0 and variance ${\sigma_{\Delta t}}^2$. We defined the Inter-Pairing-Interval (IPI) as the time interval between the presynaptic stimulation times of two consecutive paired stimulations ($\mathrm{IPI}_i = t_{\mathrm{pre}_{i+1}} - t_{\mathrm{pre}_i}$), whereas the spike timing Δt is the time interval between the postsynaptic and the presynaptic stimulation times within a given paired stimulation ($\Delta t_{\mathrm{STDP}_i} = t_{\mathrm{post}_i} - t_{\mathrm{pre}_i}$). In a standard STDP protocol both the spike timing and the IPI are constant. The above algorithm yields constant IPIs and stochastic spike timings.

Electrophysiological data analysis

Off-line analysis was performed with Fitmaster (Heka Elektronik) and Igor-Pro 6.0.3 (Wavemetrics). Statistical analysis was performed with Prism 5.02 software. In all cases "n" refers to an experiment on a single cell from a single slice. All results are expressed as mean ± SEM in the text and as mean±SD in the figures. Statistical significance was assessed in unpaired *t* tests, one way ANOVA, or in one-sample *t* tests, as appropriate, using the indicated significance threshold (*p*).

Mathematical model

Jittered STDP protocols. In the model, we define the spike timing as $\Delta t_{\mathrm{STDP}_i} = t_{\mathrm{post}_i} - t_{\mathrm{pre}_i} + \delta$ where δ accounts for the time elapsed between the onset of the postsynaptic step current and the action potential it triggers (~3ms in MSNs). In agreement with the experiment protocol above, we introduced stochasticity of the spike timing by adding a random jitter $\xi_{\Delta t}$ to the spike timing: $\Delta t_{\mathrm{STDP}} = m_{\Delta t} + \xi_{\Delta t}$, were $m_{\Delta t}$ is the average spike timing and $\xi_{\Delta t}$ is a random variable whose distribution is given by the STDP protocol. Here, we explored five STDP protocols:

1) *Protocol 0* consisted of pairings with no jittering, i.e. $\mathrm{IPI}_i = \frac{1}{F_{\mathrm{pairings}}}$ and $\xi_{\Delta t} = 0$.

2) *Protocol 1* consisted of deterministic IPIs and uniformly distributed spike timings (Fig. 2a1), i.e. $\mathrm{IPI}_i = \frac{1}{F_{\mathrm{pairings}}}, \forall i$, and the probability distribution function of the jitter is given by

$$P(\xi_{\Delta t}) = \begin{cases} \frac{1}{2\sigma_{\Delta t}} & \text{if } |\xi_{\Delta t}| < \sigma_{\Delta t}, \\ 0 & \text{otherwise} \end{cases} \quad (1)$$

In eq. (1), $\sigma_{\Delta t}$ defines the maximal jitter amplitude *i.e.* the level of noise in the protocol. To simulate *Protocol 1*, we first set each presynaptic stimulation time using $t_{\mathrm{pre}_i} = \frac{i}{F_{\mathrm{pairings}}}$. Postsynaptic times were then fixed by $t_{\mathrm{post}_i} = t_{\mathrm{pre}_i} + m_{\Delta t} + \xi_{\Delta t,i} - \delta$.

3) *Protocol 2* (Fig. 2c1) shared the same definition as Protocol 1, except that the jitter followed a normal distribution with zero mean and variance ${\sigma_{\Delta t}}^2$: $P(\xi_{\Delta t}) = \mathcal{N}(0, {\sigma_{\Delta t}}^2)$.

4) For *Protocol 3* (Fig. 2d1), we used a triangular distribution of the jitter by adding uniformly distributed jitter to both presynaptic and postsynaptic times. We set $t_{\mathrm{pre}_i} = \frac{i}{F_{\mathrm{pairings}}} + \zeta_{\mathrm{pre},i}$ and $t_{\mathrm{post}_i} = \frac{i}{F_{\mathrm{pairings}}} + m_{\Delta t} + \zeta_{\mathrm{post},i} - \delta$, where ζ_{pre} and ζ_{post} are i.i.d.

511 random variables with the uniform distribution of eq. (1). The resulting spike timing is
512 $\Delta t_{\mathrm{STDP}} = m_{\Delta t} + \xi_{\Delta t}$ where $\xi_{\Delta t} = \zeta_{\mathrm{post}} - \zeta_{\mathrm{pre}}$ has a triangular distribution. Note that in this
513 case, one still has $\mathrm{IPI}_i \approx \frac{1}{F_{\mathrm{pairings}}}\ \forall i$ as long as $2|m_{\Delta t}|F_{\mathrm{pairings}} \ll 1$, which can safely be
514 assumed here since we used $|m_{\Delta t}| < 50\mathrm{ms}$ and $F_{\mathrm{pairings}} < 2\mathrm{Hz}$.

515 5) *Protocol 4* includes both a stochastic spike timing and stochastic IPIs (Fig. 2e1). We first
516 sampled N_{pairings} IPIs according to an exponential distribution with rate λ and refractory
517 period τ_r: $P(\mathrm{IPI}) = \Theta(\mathrm{IPI} - \tau_r)\lambda\exp(-\lambda(\mathrm{IPI} - \tau_r))$, where $\Theta(x)$ is the Heaviside function
518 $\Theta(x)=1 \text{if } x \geq 0; 0 \text{ otherwise}$. The spike trains defined with protocol 4 are thus Poisson
519 process. We used these IPIs to fix the stimulation times, adding a triangularly distributed jitter
520 as in Protocol 3 above: $t_{\mathrm{pre}_i} = \sum_{j<i} \mathrm{IPI}_j + \zeta_{\mathrm{pre},i}$ and $t_{\mathrm{post}_i} = \sum_{j<i} \mathrm{IPI}_j + m_{\Delta t} + \zeta_{\mathrm{post},i} - \delta$.
521 To keep the average stimulation frequency at $1/F_{\mathrm{pairings}}$, we constrained the value of the rate
522 λ as $\lambda = \left(1/F_{\mathrm{pairings}} - \tau_r\right)^{-1}$.

523
524 **Stimulations**. A detailed account of our mathematical model can be found in S1 Text. We
525 modeled glutamate concentration in the synaptic cleft, $G(t)$, as a train of exponentially-
526 decaying impulses triggered by presynaptic stimuli at time t_{pre_i}. We modeled the electrical
527 response to these stimulations in a postsynaptic element considered as a single isopotential
528 compartment with AMPAR, NMDAR, VSCC and TRPV1 conductances:

529
$$\begin{aligned} C_{\mathrm{m}}\, dV/dt \quad &= -g_L(V - V_{\mathrm{L}}) - I_{\mathrm{AMPAR}}(V, G(t)) - I_{\mathrm{NMDAR}}(V, G(t)) \\ &\quad -I_{\mathrm{VSCC}}(V) - I_{\mathrm{TRPV1}}(V, AEA) - I_{\mathrm{action}}(t) \end{aligned} \qquad (2)$$

530 where V is membrane potential; g_{L} and V_{L} are leak conductance and reversal potential
531 respectively; I_{AMPAR}, I_{NMDAR}, I_{VSCC} and I_{TRPV1} are currents through AMPAR, NMDAR, L-
532 type VSCC (v1.3) and TRPV1 respectively. I_{action} is the action current resulting from the

postsynaptic stimulation (backpropagating action potential on top of a 30ms depolarization). Details about the analytical expressions of these currents are given in S1 Text.

Biochemical signaling. We modeled the kinetics of the biochemical pathways activated by the above electrical stimulations using the model of ref[13]. We give below a quick overview of this model and refer to S1 Text for the details. Free cytosolic calcium is one of the main signaling actors in the model. To model its dynamics, we assumed calcium can be transferred from/to two main sources: (*i*) extracellular calcium, via the plasma membrane channels of eq. (3) above and (*ii*) the endoplasmic reticulum (ER), via the IP3-dependent calcium-induced calcium release system. These calcium transients activated a network of biochemical pathways that collectively set the synaptic weight. Hence, in this model, the synaptic weight is entirely fixed by the underlying biochemical signaling network[13]. More precisely, we assumed that the total synaptic weight is the product of a pre- and a postsynaptic contribution $W_{\mathrm{total}} = W_{\mathrm{pre}} W_{\mathrm{post}}$. Postsynaptic plasticity was based on the activation by calcium of calmodulin and CaMKII[67,68]. We assumed that postsynaptic plasticity is directly proportional to the calcium-dependent activation of CaMKII:

$$W_{\mathrm{post}} = 1 + 3.5 \frac{CaMKII^*}{CaMKII^*_{\mathrm{max}}} \qquad (5)$$

where $CaMKII^*$ and $CaMKII^*_{\mathrm{max}}$ are the current concentration of activated (phosphorylated) CaMKII and its maximum value.

Our model also accounts for the biochemical pathways leading to the production of the endocannabinoids 2-arachidonoylglycerol (2-AG) and AEA, and their subsequent activation of CB_1R (see S1 Text for further details). In our model, CB_1R activation (y_{CB1R}) controls the presynaptic weight W_{pre} according to the following rule:

555 $$\Omega(y_{\mathrm{CB1R}}) = \begin{cases} 1 - A_{\mathrm{LTD}} & \text{if } \Theta_{\mathrm{LTD}}^{\mathrm{start}} < y_{\mathrm{CB1R}} < \Theta_{\mathrm{LTD}}^{\mathrm{stop}} \\ 1 + A_{\mathrm{LTP}} & \text{if } \Theta_{\mathrm{LTP}}^{\mathrm{start}} < y_{\mathrm{CB1R}} \\ 1 & \text{otherwise} \end{cases} \quad (7)$$

556 $$\text{and } \mathrm{d}W_{\mathrm{pre}}/\mathrm{d}t = \left(\Omega(y_{\mathrm{CB1R}}) - W_{\mathrm{pre}}\right)/\tau_{W_{\mathrm{pre}}} \quad (8)$$

557 Details about model implementation and numerics are given in the supplementary
558 information.

Acknowledgments: We thank the LV lab members for helpful suggestions and critical comments, in particular Sebastien Valverde for proofreading of the manuscript. This work was supported by grants from INSERM, Collège de France, the Agence Nationale pour la Recherche (Grant Dopaciumcity ANR-14-NEUC-0003), INRIA, CNRS, and the Ecole des Neurosciences de Paris.

Author contribution:

L.V. and H.B. designed the study; Y.C. and A.M. performed electrophysiological experiments and analysis; H.B. carried out the conception and the design of the mathematical model; H.B. and I.P. performed the acquisition and analysis of data from the mathematical model; H.B. and L.V. wrote the manuscript and all authors have edited and corrected the manuscript; L.V. supervised the whole study.

Competing financial interest:

The authors declare no competing interests.

Figure Legends

Figure 1: NMDAR- and eCB-mediated STDP induced with fixed Δt_{STDP}

(**a**) STDP protocol: a single postsynaptic spike was paired with a single cortical stimulation, 10 or 100 times at 1Hz. (**b**) Example of 5 successive pairings (#4-8, from c1) exhibiting relatively fixed Δt_{STDP} (#4-8: -8.0, -7.8, -7.4, -8.8 and -8.0ms). Plotting the successive Δt_{STDP} illustrates their low variance $\sigma_{\Delta t}$ (2.6ms). (**c**) Corticostriatal NMDAR-mediated tLTP induced by 100 post-pre pairings with fixed Δt_{STDP}. (**c1**) Example of tLTP induced by 100 post-pre pairings ($m_{\Delta t}$=-9ms, $\sigma_{\Delta t}$=2.6ms). The mean baseline EPSC amplitude, 95±3pA, increased by 77% to 168±6pA 45 minutes after pairings. Upper panel, time course of Ri (baseline: 172±2MΩ and 35-45 min after pairings: 170±3MΩ; change of 1%) and holding current (I_{hold}). Inset: distribution of the 100 Δt_{STDP}. (**c2**) Averaged time-courses of tLTP induced by 100 post-pre pairings; this tLTP was NMDAR-mediated because prevented by D-AP5 (50µM). (**c3**) Relationship between the STDP magnitude and the STDP jitter for each of the recorded neurons. (**d**) Corticostriatal eCB-mediated t-LTD induced by 100 pre-post pairings with fixed Δt_{STDP}. (**d1**) Example of tLTD induced by 100 pre-post pairings ($m_{\Delta t}$=+21ms, $\sigma_{\Delta t}$=2.1ms); the mean baseline EPSC amplitude, 206±4pA, decreased by 25%, to 154±8pA, 45 minutes after pairings. Upper panel, time course of Ri (baseline: 195±1MΩ and 45-55 min after pairings: 196±2MΩ; change <1%) and I_{hold}. Inset: distribution of the 100 Δt_{STDP}. (**d2**) Averaged time-courses of tLTD induced by 100 pre-post pairings; this tLTD was CB_1R-mediated because prevented by AM251 (3µM). (**d3**) Relationship between the STDP magnitude and the jitter. (**e**) Corticostriatal eCB-mediated tLTP induced by 10 post-pre pairings with fixed Δt_{STDP}. (**e1**) Example of tLTP induced by 10 post-pre pairings ($m_{\Delta t}$=-11ms, $\sigma_{\Delta t}$=3.1ms); the mean baseline EPSC amplitude, 147±3pA, increased by 43% to 209±9pA 45 minutes after pairings. Upper panel, time course of Ri (baseline: 227±2MΩ and 45-55 min after pairings: 239±2MΩ; change of 5%) and I_{hold}. Inset: distribution of the 10

600 Δt_{STDP}. (**e2**) Averaged time-courses of tLTP induced by 10 post-pre pairings; this tLTP was
601 CB_1R-mediated because prevented by AM251. (**e3**) Relationship between the STDP
602 magnitude and the jitter. (**c1**-**d1**-**e1**) Insets: average of 12 successive EPSC amplitude at
603 baseline (black traces) and at 40-50 min after pairings (grey traces). (**f**) Predictions of the
604 mathematical model in the absence of added jitter. The model expresses the biochemical
605 pathways schematized in (**f1**). (**f2**) Changes of W_{total} with various Δt_{STDP} and $N_{pairings}$. (**f3**)
606 Removing NMDAR/CaMKII signaling suppresses the tLTP observed for $\Delta t_{STDP}>0$ and
607 $N_{pairings}>50$. (**f4**) Removing CB_1R suppresses the tLTP observed for $\Delta t_{STDP}>0$ and $N_{pairings}<20$
608 and the tLTD observed for $\Delta t_{STDP}<0$.
609
610 **Figure 2: The mathematical model predicts that NMDAR-tLTP is less robust to jitter**
611 **than eCB-tLTP and eCB-tLTD.**

612 (**a**) Using a jittered STDP protocol combining uniformly-distributed jitter of the spike timing
613 with deterministic IPIs at 1Hz (**a1**), the amplitudes of NMDAR-tLTP, eCB-tLTD and eCB-
614 tLTP decrease with increasing jitter amplitudes $\sigma_{\Delta t}$ (**a2**). eCB-tLTP (red full line) was
615 triggered with 10 pairings of average spike timing $m_{\Delta t} = -15$ms and eCB-tLTD (blue full
616 line) with 100 pairings of $m_{\Delta t} = +20$ms. NMDAR-tLTP (red dashed line) corresponded to
617 100 pairings of $m_{\Delta t} = -15$ms. eCB-tLTD and eCB-tLTP are weakly affected by the jitter.
618 NMDAR-tLTP is less robust. Full and dashed lines show averages and light swaths show
619 ±1sem. (**b**) Evolution of NMDAR-tLTP, eCB-tLTD and eCB-tLTP domains for $\sigma_{\Delta t} = 0$ (**b1**),
620 5 (**b2**) and 10ms (**b3**) for the STDP protocol of (**a**). Note the persistence of the eCB-tLTD
621 domain (blue box) while eCB-tLTP (red box) and NMDAR-tLTP domain (red dashed box)
622 disappeared for 5 and 10ms, respectively. (**c**-**e**) Similar results are obtained with other jitter
623 distributions, including Gaussian-distributed jitter (**c**) and triangularly-distributed jitter (**d**).
624 We also considered a combination of triangularly-distributed jitter with random IPIs

distributed according to an exponential distribution with refractory period τ_r=0.95 s (see *Methods*) in (**e**). The plots of the amplitude of NMDAR-tLTP, eCB-tLTD and eCB-tLTP for increasing jitter amplitude $\sigma_{\Delta t}$ (**c2, d2, e2**) show similar profiles and are similar to panel (**a2)**, indicating that the model predictions are not qualitatively modified by the probability distribution function of the jitter.

Figure 3: Differential effect of jitter on NMDAR- and eCB-mediated plasticity.

(a) STDP protocol; Δt_{STDP} indicates the time between pre- and postsynaptic stimulations. Δt_{STDP} <0 and Δt_{STDP} >0 refer to post-pre and pre-post pairings, respectively. (**b**) Example of 5 successive pairings (#5-9, from c1) exhibiting jittered values of Δt_{STDP} (#5-9: -10.3, -15.2, -30.5, -20.7 and -17.3ms); these pairings are indicated with the grey frame within the 100 pairings displaying jittered Δt_{STDP}. The distribution of the successive Δt_{STDP} illustrate their standard deviation $\sigma_{\Delta t}$=7.9ms. (**c**) NMDAR-tLTP is prevented with $\sigma_{\Delta t}$>3ms. (**c1**) Example of the absence of plasticity after 100 post-pre pairings with $m_{\Delta t}$=-18ms and $\sigma_{\Delta t}$=7.9ms; the mean baseline EPSC amplitude, 194±3pA, did not show significant change 45 minutes after pairing, 186±4pA. Upper panel, time course of Ri (baseline: 198±2MΩ and 45-55 min after pairings: 194±2MΩ; change of 2%) and holding current (I_{hold}). Inset: distribution of the 100 Δt_{STDP}. (**c2**) Averaged time-courses of the absence of plasticity after 100 post-pre pairings with 3<$\sigma_{\Delta t}$<10ms. (**c3**) Relationship between the STDP magnitude and the jitter. (**d**) eCB-mediated t-LTD is not affected by 3<$\sigma_{\Delta t}$<10ms. (**d1**) Example of tLTD induced by 100 pre-post pairings with $m_{\Delta t}$ =+18ms and $\sigma_{\Delta t}$ =7.1ms; the mean baseline EPSC amplitude, 160±3pA, decreased by 50%, to 81±5pA, 45 minutes after pairings. Upper panel, time course of Ri (baseline: 112±1MΩ and 35-45 min after pairings: 118±1MΩ; change of 5%) and I_{hold}. Inset: distribution of the 100 Δt_{STDP}. (**d2**) Averaged time-courses of tLTD induced by 100 pre-post pairings with 3<$\sigma_{\Delta t}$<10ms. (**d3**) Relationship between the STDP magnitude and the

jitter. (**e**) eCB-mediated tLTP is not affected by 3<$\sigma_{\Delta t}$<10ms. (**e1**) Example of tLTP induced by 10 post-pre pairings with $m_{\Delta t}$=-21ms and $\sigma_{\Delta t}$=6.4ms; the mean baseline EPSC amplitude, 113±2 pA, increased by 115% to 243±6pA 45 minutes after pairings. Upper panel, time course of Ri (baseline: 185±1MΩ and 45-55 min after pairings: 197±2MΩ; change of 6%) and I_{hold}. Inset: distribution of the 10 Δt_{STDP}. (**e2**) Averaged time-courses of tLTP induced by 10 post-pre pairings with 3<$\sigma_{\Delta t}$<10ms. (**e3**) Relationship between the STDP magnitude and the jitter.

Insets: average of 12 successive EPSC amplitude at baseline (black trace) and at 40-50 min after STDP pairings (grey trace). Error bars represent the SEM.

Figure 4: Model-based analysis of the effects of jittering.

Model-predicted time-courses of (**a**) CB_1R activation y_{CB1R} and (**b**) the concentration of active CaMKII during a protocol with jitter amplitude $\sigma_{\Delta t} = 0$ (**a1**-**b1**), 5 (**a2**-**b2**) or 10 (**a3**-**b3**) ms. The STDP protocol was the same as Figure 2a1 *i.e.* uniformly-distributed jitter of the spike timing and deterministic IPIs at 1Hz. eCB-tLTP (**a**, red full line) and NMDAR-tLTP (**b**, red dashed line) were triggered with average spike timing $m_{\Delta t} = -15$ms and eCB-tLTD (**a**, blue full line) with $m_{\Delta t} = +20$ms. In (**a**) the shaded boxes locate the areas where y_{CB1R} triggers eCB-tLTP or eCB-tLTD. Those areas are defined by the thresholds θ_{LTP}^{start} and (θ_{LTD}^{start}, θ_{LTD}^{stop}), respectively (see *Methods*). For $m_{\Delta t} = -15$ ms (red), increasing jitter amplitudes progressively hinders the build up of the y_{CB1R} transients. y_{CB1R} still reaches the LTP area for 5-25 pairings with $\sigma_{\Delta t} = 0$ (**a1**) and 5ms (**a2**) thus triggering eCB-tLTP but fails to do so for $\sigma_{\Delta t} = 10$ms (**a3**). Conversely, eCB-tLTD is robust to jitter because y_{CB1R} remains in the LTD region for most of the pairings with $m_{\Delta t} = +20$ms (blue), for all tested jitter amplitudes. In (**b**), with $m_{\Delta t} = -15$ms (red) the switch from the low activation to the high activation state

674 of CaMKII is obtained in the absence of jittering $\sigma_{\Delta t} = 0$ms (**b1**). The progressive build up of
675 activated CaMKII is efficiently suppressed as soon as $\sigma_{\Delta t} = 5$ms (**b2**) thus effectively
676 suppressing NMDAR-tLTP (**b3**).
677
678 **Figure 5: Model-based analysis of the change of robustness with frequency.**
679 **(a)** Summary of the robustness of the model plasticity at 1Hz. The jittered STDP protocol
680 combined uniformly-distributed jitter of the spike timing and constant IPIs at 1Hz. Two-
681 dimensional maps show alterations of the plasticity obtained with 10 (**a1**) or 100 (**a2**)
682 pairings, when the average spike timing $m_{\Delta t}$ and the jitter amplitude $\sigma_{\Delta t}$ are changed. The
683 locations of the plasticity blotches are indicated with horizontal lines: full red for eCB-tLTP,
684 full blue for eCB-tLTD and dashed red for NMDAR-tLTP. The length of each of these
685 blotches along the y-axis reflects their robustness to jitter. (**a3**) A cross-section along the
686 dashed and full horizontal lines of (**a1**-**a2**) illustrates the robustness of NMDAR-tLTP, eCB-
687 tLTD and eCB-tLTP. (**b**) Robustness of the model with larger frequency (1.05Hz) and same
688 jittered STDP protocol as in (**a**). Note the distortion between the pairing frequency in the
689 model and in the experiments. The behavior of the model for F_{pairings}=1.05Hz corresponds to
690 experimental results with F_{pairings} ≈3Hz[13]. The two-dimensional maps for 10 (**b1**) or 100 (**b2**)
691 pairings as well as the cross-sections (**b3**) predict that for frequencies larger than 1Hz, the
692 robustness changes, with NMDAR-tLTP becoming more robust.
693
694 **Figure 6: Increasing frequency and N_{pairings} stabilized NMDAR-tLTP against jitter.**

695 (**a**) 100 post-pre pairings at 3Hz induced a tLTP, which is not affected by 3<$\sigma_{\Delta t}$<10ms. (**a1**)
696 Example of tLTP induced by 100 post-pre pairings at 3Hz with $m_{\Delta t}$=-22ms and $\sigma_{\Delta t}$ =9ms;
697 the mean baseline EPSC amplitude, 194±4pA, increased by 212%, to 606±7pA, 45 min after
698 pairings. Upper panel, time course of Ri (baseline: 123±1MΩ and 45-55 min after pairings:

138±1MΩ; change of 12%) and I_{hold} for this cell. Inset: distribution of Δt_{STDP} for the 100 pairings. (**a2**) Averaged time-courses of tLTP induced by 100 post-pre pairings at 3Hz with $3<\sigma_{\Delta t}<10$ms. (**a3**) Relationship between the STDP magnitude and the jitter for each of the recorded neurons after 100 pairings at 1Hz (n=7; blue circles) or at 3Hz (n=10; red circles). (**b**) 250-300 post-pre pairings induced tLTP, which is not affected by $3<\sigma_{\Delta t}<10$ms. (**b1**) Example of tLTP induced by 250 post-pre pairings with $m_{\Delta t}$=-20ms and $\sigma_{\Delta t}$=5ms; the mean baseline EPSC amplitude, 126±3pA, increased by 57% to 198±4pA 45 minutes after pairings. Upper panel, time course of Ri (baseline: 65±1MΩ and 45-55 min after pairings: 65±2MΩ; change <1%) and I_{hold}. Inset: distribution of Δt_{STDP} for the 250 pairings. (**b2**) Averaged time-courses of tLTP induced by 250-300 post-pre pairings with $3<\sigma_{\Delta t}<10$ms. (**b3**) Relationship between the STDP magnitude and the jitter for each of the recorded neurons after 100 (n=7; blue circles), 200 (n=6; black circles) or 250-300 (n=7; red circles) post-pre pairings.
Insets: average of 12 successive EPSC amplitude at baseline (black trace) and at 40-50 min after STDP pairings (grey trace). Error bars represent the SEM.

Figure 7: The robustness of plasticity depends on the regularity of the presynaptic spike train.

The figure shows the robustness of the model plasticity (eCB-tLTP with red, eCB-tLTD with blue and NMDAR-tLTP with dashed red) with the jittered STDP protocol of figure 2e1, *i.e.* exponentially-distributed IPIs with refractory period τ_r and triangularly-distributed jitter $\xi_{\Delta t}$. From right to left, the refractory period $\tau_r$is gradually decreased. When $\tau_r \rightarrow 1/F_{\text{pairings}}$ where $F_{\text{pairings}} = 1$Hz is the average pairings frequency, one gets regular presynaptic spike trains, similar to classical STDP protocols. In this case (see e.g. $\tau_r = 0.95/F_{\text{pairings}}$), the robustness pattern is similar to the previous observations at 1Hz: eCB-STDP is robust, whereas NMDAR-tLTP is fragile. However, when $\tau_r \rightarrow 0$, the presynaptic spike train

becomes highly irregular. In this case, the robustness patterns changes totally, with NMDAR-LTP becoming the most robust, and eCB-tLTD turning into a LTP. Hence, irregular presynaptic spike trains are predicted to produce robust LTP at the expense of LTD.

REFERENCES

1. Takeuchi, T., Duszkiewicz, A. J. & Morris, R. G. M. The synaptic plasticity and memory hypothesis: encoding, storage and persistence. *Philos. Trans. R. Soc. Lond., B, Biol. Sci.* **369,** 20130288 (2014).
2. Debanne, D., Gähwiler, B. H. & Thompson, S. M. Bidirectional associative plasticity of unitary CA3-CA1 EPSPs in the rat hippocampus in vitro. *J. Neurophysiol.* **77,** 2851–2855 (1997).
3. Magee, J. C. & Johnston, D. A synaptically controlled, associative signal for Hebbian plasticity in hippocampal neurons. *Science* **275,** 209–213 (1997).
4. Markram, H., Lübke, J., Frotscher, M. & Sakmann, B. Regulation of synaptic efficacy by coincidence of postsynaptic APs and EPSPs. *Science* **275,** 213–215 (1997).
5. Bi, G. & Poo, M. Synaptic Modifications in Cultured Hippocampal Neurons: Dependence on Spike Timing, Synaptic Strength, and Postsynaptic Cell Type. *J. Neurosci.* **18,** 10464–10472 (1998).
6. Zhang, L. I., Tao, H. W., Holt, C. E., Harris, W. A. & Poo, M. A critical window for cooperation and competition among developing retinotectal synapses. *Nature* **395,** 37–44 (1998).
7. Sjöström, P. J., Turrigiano, G. G. & Nelson, S. B. Rate, timing, and cooperativity jointly determine cortical synaptic plasticity. *Neuron* **32,** 1149–1164 (2001).
8. Feldman, D. E. The spike-timing dependence of plasticity. *Neuron* **75,** 556–571 (2012).
9. Madadi Asl, M., Valizadeh, A. & Tass, P. A. Dendritic and Axonal Propagation Delays Determine Emergent Structures of Neuronal Networks with Plastic Synapses. *Sci Rep* **7,** 39682 (2017).

10. Froemke, R. C., Tsay, I. A., Raad, M., Long, J. D. & Dan, Y. Contribution of individual spikes in burst-induced long-term synaptic modification. *J. Neurophysiol.* **95,** 1620–1629 (2006).

11. Wittenberg, G. M. & Wang, S. S.-H. Malleability of spike-timing-dependent plasticity at the CA3-CA1 synapse. *J. Neurosci.* **26,** 6610–6617 (2006).

12. Cui, Y. *et al.* Endocannabinoids mediate bidirectional striatal spike-timing-dependent plasticity. *J. Physiol. (Lond.)* **593,** 2833–2849 (2015).

13. Cui, Y. *et al.* Endocannabinoid dynamics gate spike-timing dependent depression and potentiation. *Elife* **5,** e13185 (2016).

14. Sjöström, P. J. & Häusser, M. A Cooperative Switch Determines the Sign of Synaptic Plasticity in Distal Dendrites of Neocortical Pyramidal Neurons. *Neuron* **51,** 227–238 (2006).

15. Clopath, C., Büsing, L., Vasilaki, E. & Gerstner, W. Connectivity reflects coding: a model of voltage-based STDP with homeostasis. *Nat. Neurosci.* **13,** 344–352 (2010).

16. Pawlak, V., Wickens, J. R., Kirkwood, A. & Kerr, J. N. D. Timing is not Everything: Neuromodulation Opens the STDP Gate. *Front Synaptic Neurosci* **2,** (2010).

17. Frémaux, N. & Gerstner, W. Neuromodulated Spike-Timing-Dependent Plasticity, and Theory of Three-Factor Learning Rules. *Front Neural Circuits* **9,** 85 (2015).

18. Valtcheva, S. & Venance, L. Astrocytes gate Hebbian synaptic plasticity in the striatum. *Nat Commun* **7,** (2016).

19. Froemke, R. C. & Dan, Y. Spike-timing-dependent synaptic modification induced by natural spike trains. *Nature* **416,** 433–438 (2002).

20. Celikel, T., Szostak, V. A. & Feldman, D. E. Modulation of spike timing by sensory deprivation during induction of cortical map plasticity. *Nat. Neurosci.* **7,** 534–541 (2004).

774 21. Morrison, A., Diesmann, M. & Gerstner, W. Phenomenological models of synaptic
775 plasticity based on spike timing. *Biol Cybern* **98,** 459–478 (2008).
776 22. Pawlak, V., Greenberg, D. S., Sprekeler, H., Gerstner, W. & Kerr, J. N. D. Changing
777 the responses of cortical neurons from sub- to suprathreshold using single spikes in vivo.
778 *Elife* **2,** e00012 (2013).
779 23. Abbott, L. F. & Nelson, S. B. Synaptic plasticity: taming the beast. *Nat. Neurosci.* **3**
780 **Suppl,** 1178–1183 (2000).
781 24. Graupner, M., Wallisch, P. & Ostojic, S. Natural Firing Patterns Imply Low
782 Sensitivity of Synaptic Plasticity to Spike Timing Compared with Firing Rate. *J. Neurosci.*
783 **36,** 11238–11258 (2016).
784 25. Sjöström, P. J., Turrigiano, G. G. & Nelson, S. B. Neocortical LTD via coincident
785 activation of presynaptic NMDA and cannabinoid receptors. *Neuron* **39,** 641–654 (2003).
786 26. Bender, V. A., Bender, K. J., Brasier, D. J. & Feldman, D. E. Two Coincidence
787 Detectors for Spike Timing-Dependent Plasticity in Somatosensory Cortex. *J Neurosci* **26,**
788 4166–4177 (2006).
789 27. Nevian, T. & Sakmann, B. Spine Ca2+ signaling in spike-timing-dependent plasticity.
790 *J. Neurosci.* **26,** 11001–11013 (2006).
791 28. Banerjee, A. *et al.* Double dissociation of spike timing-dependent potentiation and
792 depression by subunit-preferring NMDA receptor antagonists in mouse barrel cortex.
793 *Cereb. Cortex* **19,** 2959–2969 (2009).
794 29. Fino, E. *et al.* Distinct coincidence detectors govern the corticostriatal spike timing-
795 dependent plasticity. *J. Physiol. (Lond.)* **588,** 3045–3062 (2010).
796 30. Sjöström, P. J., Rancz, E. A., Roth, A. & Häusser, M. Dendritic excitability and
797 synaptic plasticity. *Physiol. Rev.* **88,** 769–840 (2008).

798 31. Korte, M. & Schmitz, D. Cellular and System Biology of Memory: Timing,
799 Molecules, and Beyond. *Physiol. Rev.* **96,** 647–693 (2016).
800 32. Pawlak, V. & Kerr, J. N. D. Dopamine receptor activation is required for
801 corticostriatal spike-timing-dependent plasticity. *J. Neurosci.* **28,** 2435–2446 (2008).
802 33. Shen, W., Flajolet, M., Greengard, P. & Surmeier, D. J. Dichotomous dopaminergic
803 control of striatal synaptic plasticity. *Science* **321,** 848–851 (2008).
804 34. Paille, V. *et al.* GABAergic circuits control spike-timing-dependent plasticity. *J.*
805 *Neurosci.* **33,** 9353–9363 (2013).
806 35. Valtcheva, S. *et al.* Developmental control of spike-timing-dependent plasticity by
807 tonic GABAergic signaling in striatum. *Neuropharmacology* **121,** 261–277 (2017).
808 36. Fino, E., Glowinski, J. & Venance, L. Bidirectional activity-dependent plasticity at
809 corticostriatal synapses. *J. Neurosci.* **25,** 11279–11287 (2005).
810 37. Schulz, J. M., Redgrave, P. & Reynolds, J. N. J. Cortico-striatal spike-timing
811 dependent plasticity after activation of subcortical pathways. *Front Synaptic Neurosci* **2,** 23
812 (2010).
813 38. Graupner, M. & Brunel, N. STDP in a Bistable Synapse Model Based on CaMKII and
814 Associated Signaling Pathways. *PLOS Computational Biology* **3,** e221 (2007).
815 39. Goubard, V., Fino, E. & Venance, L. Contribution of astrocytic glutamate and GABA
816 uptake to corticostriatal information processing. *J. Physiol. (Lond.)* **589,** 2301–2319
817 (2011).
818 40. Markram, H., Wang, Y. & Tsodyks, M. Differential signaling via the same axon of
819 neocortical pyramidal neurons. *PNAS* **95,** 5323–5328 (1998).
820 41. Fino, E., Deniau, J.-M. & Venance, L. Cell-specific spike-timing-dependent plasticity
821 in GABAergic and cholinergic interneurons in corticostriatal rat brain slices. *J. Physiol.*
822 *(Lond.)* **586,** 265–282 (2008).

823 42. Froemke, R. C., Poo, M.-M. & Dan, Y. Spike-timing-dependent synaptic plasticity
824 depends on dendritic location. *Nature* **434,** 221–225 (2005).
825 43. Tzounopoulos, T., Rubio, M. E., Keen, J. E. & Trussell, L. O. Coactivation of Pre- and
826 Postsynaptic Signaling Mechanisms Determines Cell-Specific Spike-Timing-Dependent
827 Plasticity. *Neuron* **54,** 291–301 (2007).
828 44. Xu, J.-Y., Zhang, J. & Chen, C. Long-lasting potentiation of hippocampal synaptic
829 transmission by direct cortical input is mediated via endocannabinoids. *J. Physiol. (Lond.)*
830 **590,** 2305–2315 (2012).
831 45. Wang, W. *et al.* A Primary Cortical Input to Hippocampus Expresses a Pathway-
832 Specific and Endocannabinoid-Dependent Form of Long-Term Potentiation. *eNeuro* **3,**
833 ENEURO.0160-16.2016 (2016).
834 46. Zhu, P. J. & Lovinger, D. M. Persistent synaptic activity produces long-lasting
835 enhancement of endocannabinoid modulation and alters long-term synaptic plasticity. *J.*
836 *Neurophysiol.* **97,** 4386–4389 (2007).
837 47. Lin, Q.-S. *et al.* Hippocampal endocannabinoids play an important role in induction of
838 long-term potentiation and regulation of contextual fear memory formation. *Brain Res.*
839 *Bull.* **86,** 139–145 (2011).
840 48. Carlson, G., Wang, Y. & Alger, B. E. Endocannabinoids facilitate the induction of
841 LTP in the hippocampus. *Nat. Neurosci.* **5,** 723–724 (2002).
842 49. Maglio, L. E., Noriega-Prieto, J. A., Maraver, M. J. & Fernández de Sevilla, D.
843 Endocannabinoid-Dependent Long-Term Potentiation of Synaptic Transmission at Rat
844 Barrel Cortex. *Cereb. Cortex* 1–14 (2017). doi:10.1093/cercor/bhx053
845 50. Lisman, J. & Spruston, N. Questions about STDP as a General Model of Synaptic
846 Plasticity. *Front. Synaptic Neurosci.* **2,** (2010).

847 51. Sjöström, P. J., Turrigiano, G. G. & Nelson, S. B. Endocannabinoid-dependent
848 neocortical layer-5 LTD in the absence of postsynaptic spiking. *J. Neurophysiol.* **92,** 3338–
849 3343 (2004).
850 52. Fino, E., Deniau, J.-M. & Venance, L. Brief subthreshold events can act as Hebbian
851 signals for long-term plasticity. *PLoS ONE* **4,** e6557 (2009).
852 53. Brandalise, F. & Gerber, U. Mossy fiber-evoked subthreshold responses induce
853 timing-dependent plasticity at hippocampal CA3 recurrent synapses. *Proc. Natl. Acad. Sci.*
854 *U.S.A.* **111,** 4303–4308 (2014).
855 54. Dudek, S. M. & Bear, M. F. Homosynaptic long-term depression in area CA1 of
856 hippocampus and effects of N-methyl-D-aspartate receptor blockade. *Proc. Natl. Acad. Sci.*
857 *U.S.A.* **89,** 4363–4367 (1992).
858 55. Mulkey, R. M. & Malenka, R. C. Mechanisms underlying induction of homosynaptic
859 long-term depression in area CA1 of the hippocampus. *Neuron* **9,** 967–975 (1992).
860 56. Mistry, R., Dennis, S., Frerking, M. & Mellor, J. R. Dentate gyrus granule cell firing
861 patterns can induce mossy fiber long-term potentiation in vitro. *Hippocampus* **21,** 1157–
862 1168 (2011).
863 57. Perrett, S. P., Dudek, S. M., Eagleman, D., Montague, P. R. & Friedlander, M. J. LTD
864 induction in adult visual cortex: role of stimulus timing and inhibition. *J. Neurosci.* **21,**
865 2308–2319 (2001).
866 58. Massey, P. V. *et al.* Differential roles of NR2A and NR2B-containing NMDA
867 receptors in cortical long-term potentiation and long-term depression. *J. Neurosci.* **24,**
868 7821–7828 (2004).
869 59. Remy, S. & Spruston, N. Dendritic spikes induce single-burst long-term potentiation.
870 *PNAS* **104,** 17192–17197 (2007).

871 60. Holthoff, K., Kovalchuk, Y., Yuste, R. & Konnerth, A. Single-shock LTD by local
872 dendritic spikes in pyramidal neurons of mouse visual cortex. *J. Physiol. (Lond.)* **560,** 27–
873 36 (2004).
874 61. Butts, D. A., Kanold, P. O. & Shatz, C. J. A burst-based 'Hebbian' learning rule at
875 retinogeniculate synapses links retinal waves to activity-dependent refinement. *PLoS Biol.*
876 **5,** e61 (2007).
877 62. Isaac, J. T. R., Buchanan, K. A., Muller, R. U. & Mellor, J. R. Hippocampal place cell
878 firing patterns can induce long-term synaptic plasticity in vitro. *J. Neurosci.* **29,** 6840–6850
879 (2009).
880 63. Shmiel, T. *et al.* Neurons of the cerebral cortex exhibit precise interspike timing in
881 correspondence to behavior. *PNAS* **102,** 18655–18657 (2005).
882 64. London, M., Roth, A., Beeren, L., Häusser, M. & Latham, P. E. Sensitivity to
883 perturbations in vivo implies high noise and suggests rate coding in cortex. *Nature* **466,**
884 123–127 (2010).
885 65. Brette, R. Philosophy of the Spike: Rate-Based vs. Spike-Based Theories of the Brain.
886 *Front. Syst. Neurosci.* **9,** (2015).
887 66. Zuo, Y. *et al.* Complementary contributions of spike timing and spike rate to
888 perceptual decisions in rat S1 and S2 cortex. *Curr. Biol.* **25,** 357–363 (2015).
889 67. Lindskog, M., Kim, M., Wikström, M. A., Blackwell, K. T. & Kotaleski, J. H.
890 Transient calcium and dopamine increase PKA activity and DARPP-32 phosphorylation.
891 *PLoS Comput. Biol.* **2,** e119 (2006).
892 68. Fernandez, E., Schiappa, R., Girault, J.-A. & Le Novère, N. DARPP-32 is a robust
893 integrator of dopamine and glutamate signals. *PLoS Comput. Biol.* **2,** e176 (2006).
894

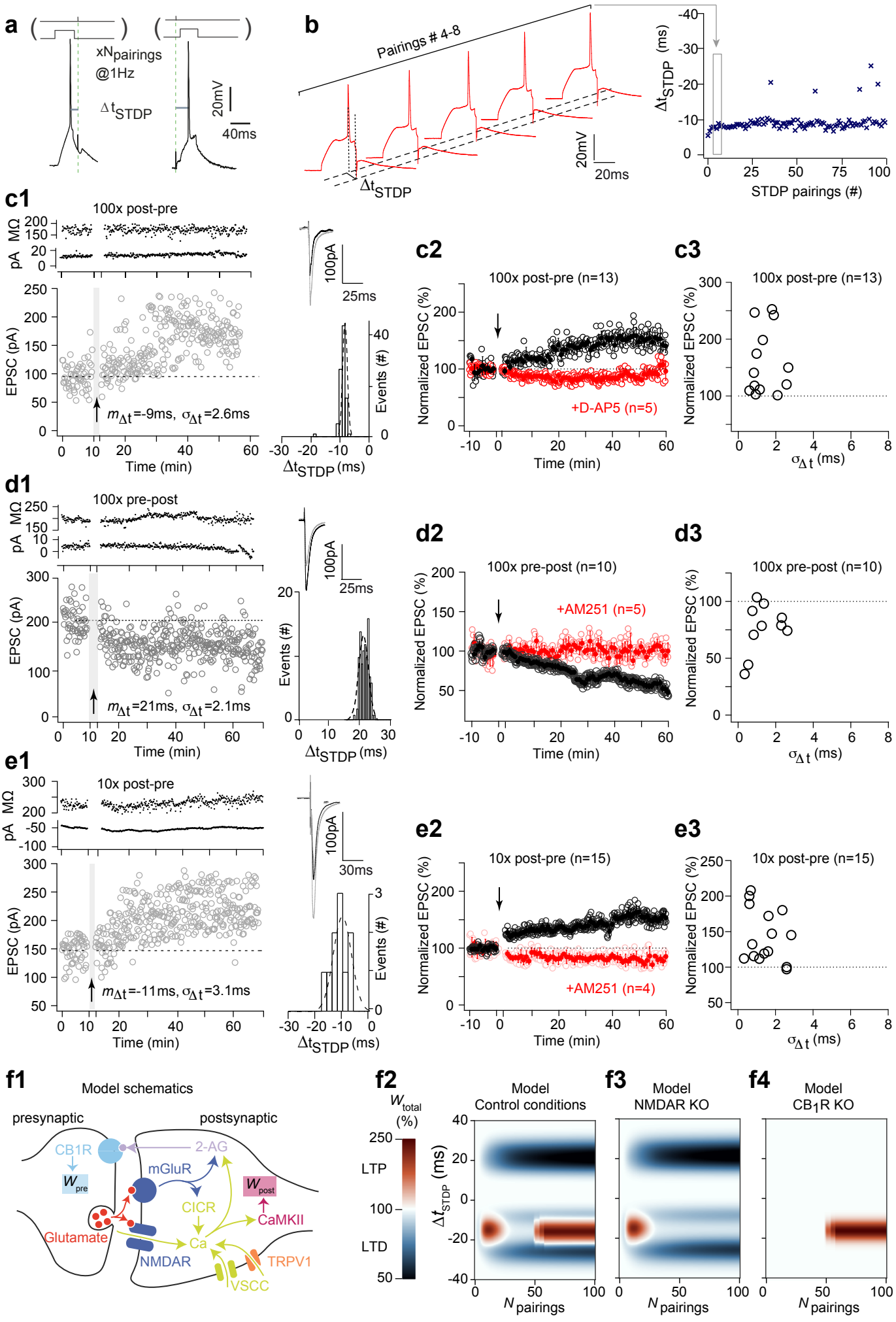
a
xNpairings
@1Hz
Δt STDP
20mV
40ms
b
Pairings # 4-8
Δt STDP
20mV
20ms
Δt STDP (ms)
STDP pairings (#)
c1
100x post-pre
MΩ
pA
EPSC (pA)
mΔt=-9ms, σΔt=2.6ms
Time (min)
100pA
25ms
Events (#)
Δt STDP (ms)
c2
100x post-pre (n=13)
Normalized EPSC (%)
+D-AP5 (n=5)
Time (min)
c3
100x post-pre (n=13)
Normalized EPSC (%)
σΔt (ms)
d1
100x pre-post
MΩ
pA
EPSC (pA)
mΔt=21ms, σΔt=2.1ms
Time (min)
100pA
25ms
Events (#)
Δt STDP (ms)
d2
100x pre-post (n=10)
+AM251 (n=5)
Normalized EPSC (%)
Time (min)
d3
100x pre-post (n=10)
Normalized EPSC (%)
σΔt (ms)
e1
10x post-pre
MΩ
pA
EPSC (pA)
mΔt=-11ms, σΔt=3.1ms
Time (min)
100pA
30ms
Events (#)
Δt STDP (ms)
e2
10x post-pre (n=15)
Normalized EPSC (%)
+AM251 (n=4)
Time (min)
e3
10x post-pre (n=15)
Normalized EPSC (%)
σΔt (ms)
f1
Model schematics
presynaptic
postsynaptic
CB1R
2-AG
mGluR
W pre
W post
CICR
CaMKII
Glutamate
Ca
NMDAR
TRPV1
VSCC
f2
W total (%)
LTP
LTD
Model
Control conditions
Δt STDP (ms)
N pairings
f3
Model
NMDAR KO
N pairings
f4
Model
CB1R KO
N pairings

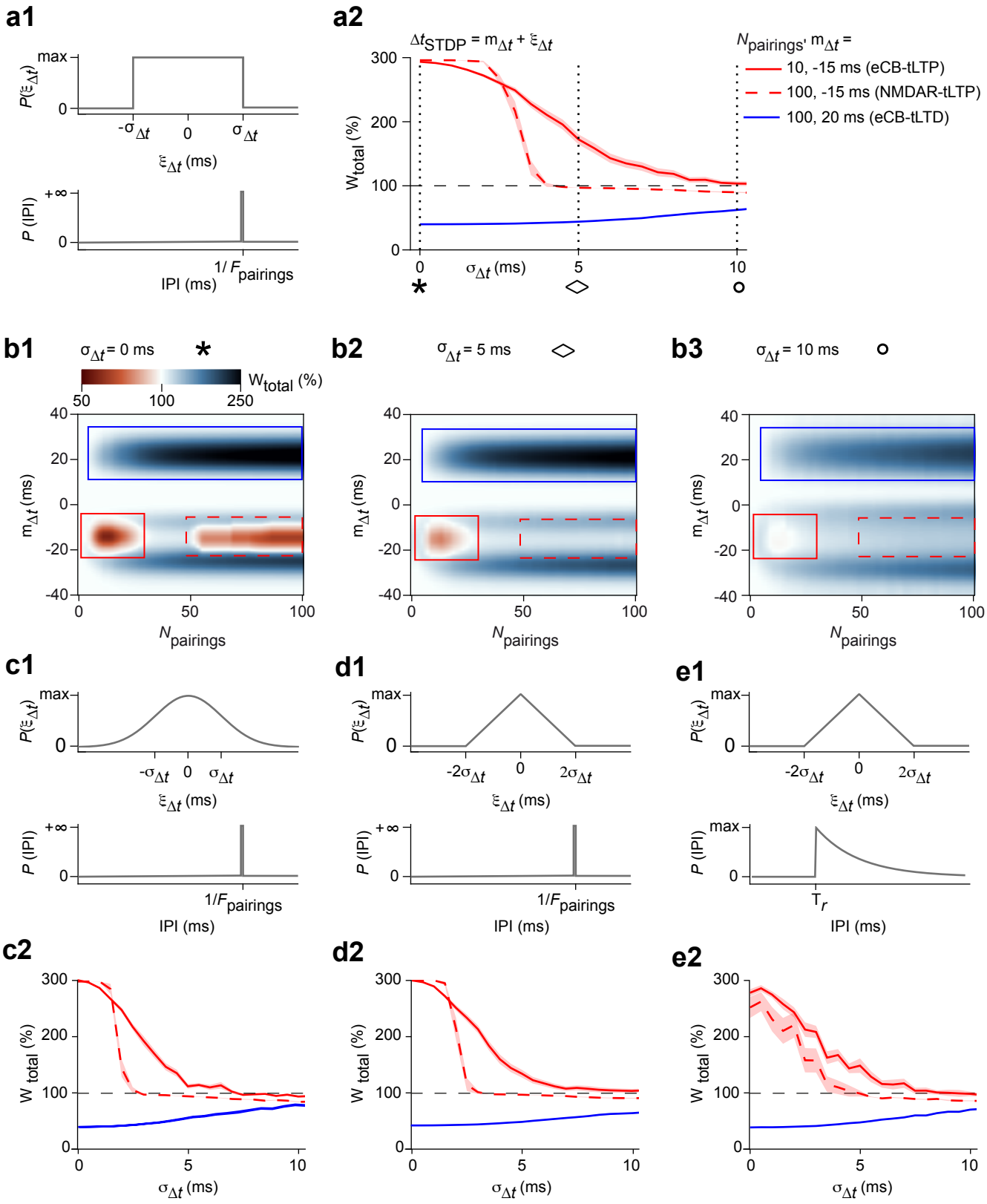
a1
a2
b1
b2
b3
c1
c2
d1
d2
e1
e2
max
0
$P(\xi_{\Delta t})$
$-\sigma_{\Delta t}$
$\sigma_{\Delta t}$
$\xi_{\Delta t}$ (ms)
P (IPI)
+∞
1/ $F_{pairings}$
IPI (ms)
$\Delta t_{STDP} = m_{\Delta t} + \xi_{\Delta t}$
$N_{pairings}$, $m_{\Delta t}$ =
10, -15 ms (eCB-tLTP)
100, -15 ms (NMDAR-tLTP)
100, 20 ms (eCB-tLTD)
W_{total} (%)
300
200
100
0
5
10
$\sigma_{\Delta t}$ (ms)
$\sigma_{\Delta t}$= 0 ms
$\sigma_{\Delta t}$= 5 ms
$\sigma_{\Delta t}$= 10 ms
50
250
40
20
-20
-40
$m_{\Delta t}$ (ms)
$N_{pairings}$
W total (%)
$-2\sigma_{\Delta t}$
$2\sigma_{\Delta t}$
$1/F_{pairings}$
T_r

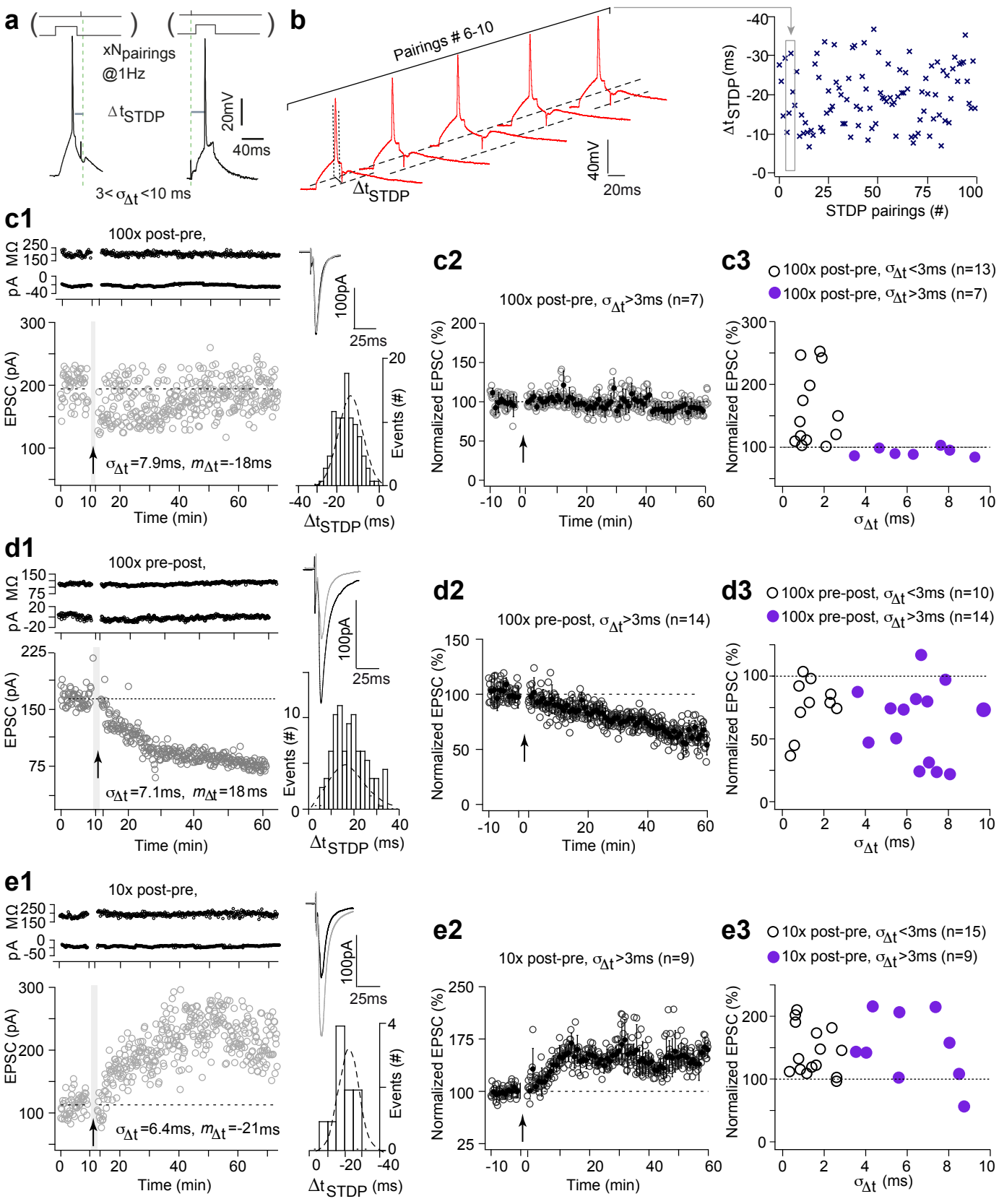
a
xNpairings
@1Hz
Δt STDP
20mV
40ms
3< σΔt <10 ms
b
Pairings # 6-10
40mV
20ms
Δt STDP
Δt STDP (ms)
STDP pairings (#)
c1
100x post-pre,
MΩ
pA
EPSC (pA)
σΔt=7.9ms, mΔt=-18ms
Time (min)
100pA
25ms
Events (#)
Δt STDP (ms)
c2
100x post-pre, σΔt>3ms (n=7)
Normalized EPSC (%)
Time (min)
c3
100x post-pre, σΔt<3ms (n=13)
100x post-pre, σΔt>3ms (n=7)
σΔt (ms)
d1
100x pre-post,
σΔt=7.1ms, mΔt=18 ms
d2
100x pre-post, σΔt>3ms (n=14)
d3
100x pre-post, σΔt<3ms (n=10)
100x pre-post, σΔt>3ms (n=14)
e1
10x post-pre,
σΔt=6.4ms, mΔt=-21ms
e2
10x post-pre, σΔt>3ms (n=9)
e3
10x post-pre, σΔt<3ms (n=15)
10x post-pre, σΔt>3ms (n=9)

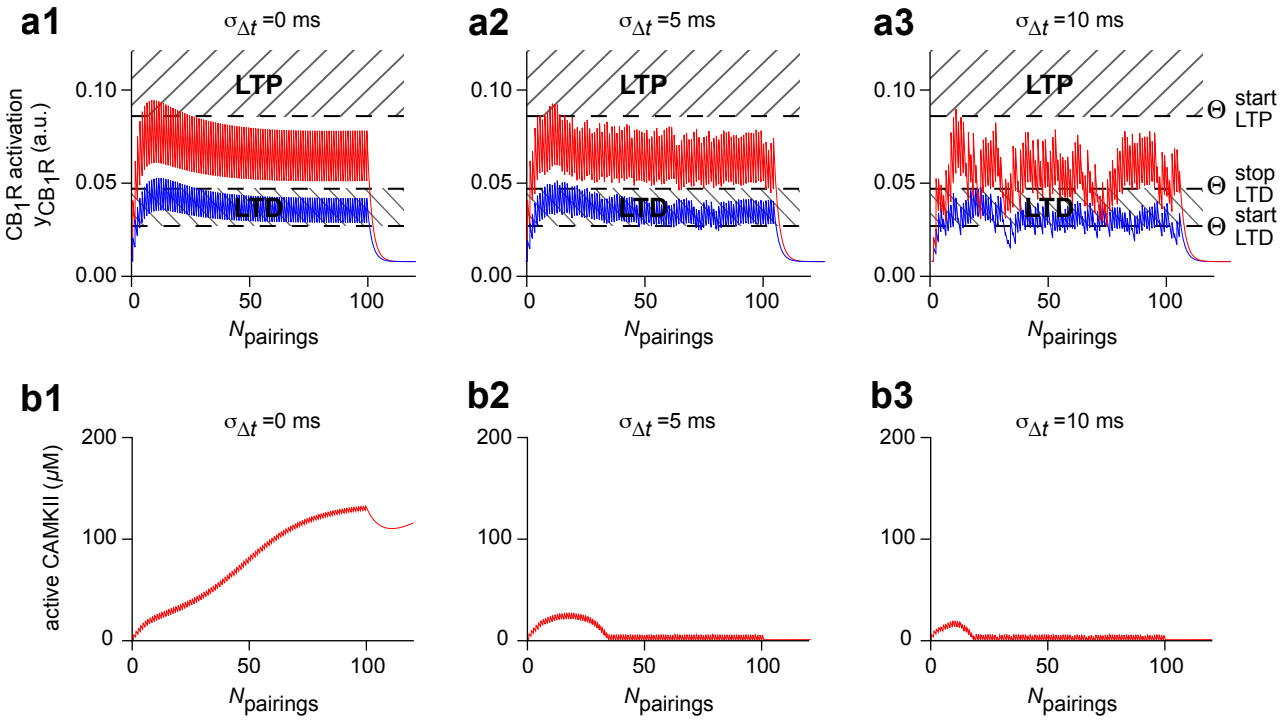
a1
σΔt =0 ms
a2
σΔt =5 ms
a3
σΔt =10 ms
LTP
LTD
Θ start LTP
Θ stop LTD
Θ start LTD
CB1R activation
yCB1R (a.u.)
0.10
0.05
0.00
0
50
100
Npairings
b1
σΔt =0 ms
b2
σΔt =5 ms
b3
σΔt =10 ms
active CAMKII (μM)
200
100
0

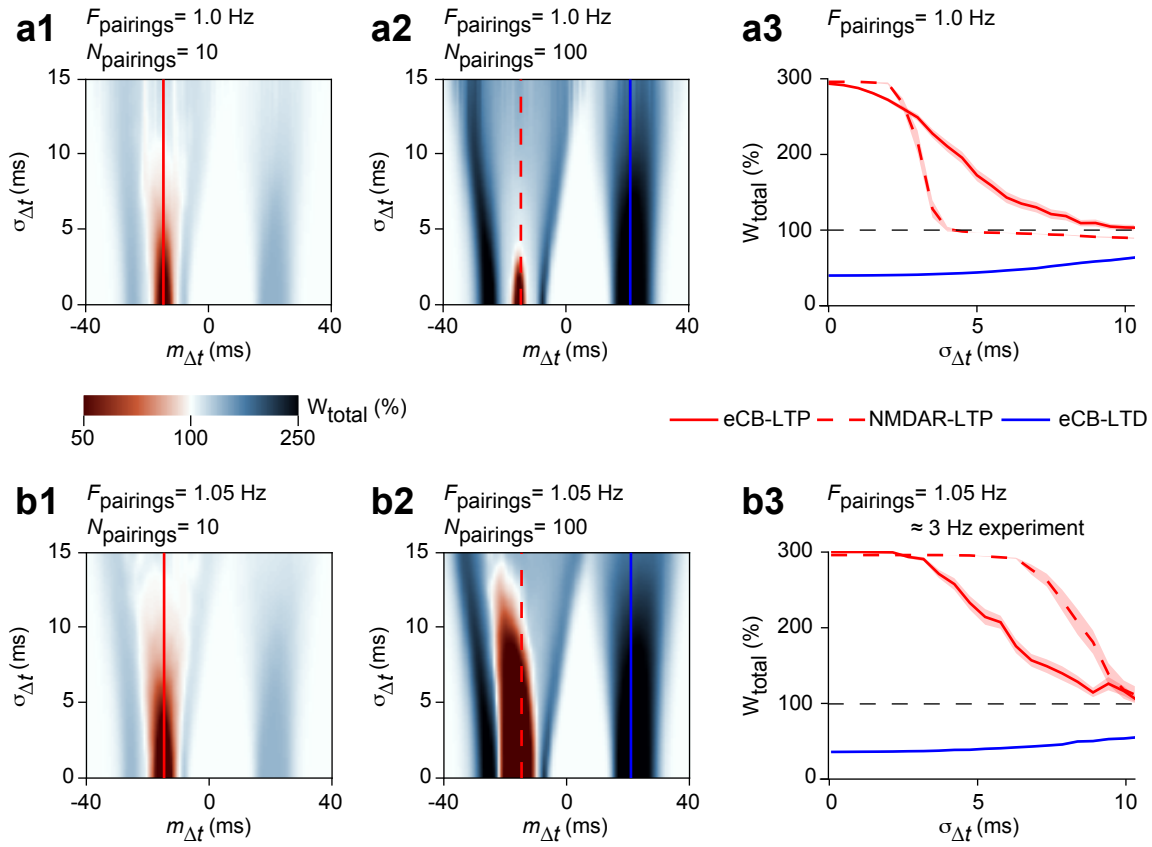
a1
$F_{pairings}$= 1.0 Hz
$N_{pairings}$= 10
a2
$F_{pairings}$= 1.0 Hz
$N_{pairings}$= 100
a3
$F_{pairings}$= 1.0 Hz
$\sigma_{\Delta t}$ (ms)
$m_{\Delta t}$ (ms)
W_{total} (%)
50
100
250
eCB-LTP
NMDAR-LTP
eCB-LTD
b1
$F_{pairings}$= 1.05 Hz
$N_{pairings}$= 10
b2
$F_{pairings}$= 1.05 Hz
$N_{pairings}$= 100
b3
$F_{pairings}$= 1.05 Hz
≈ 3 Hz experiment

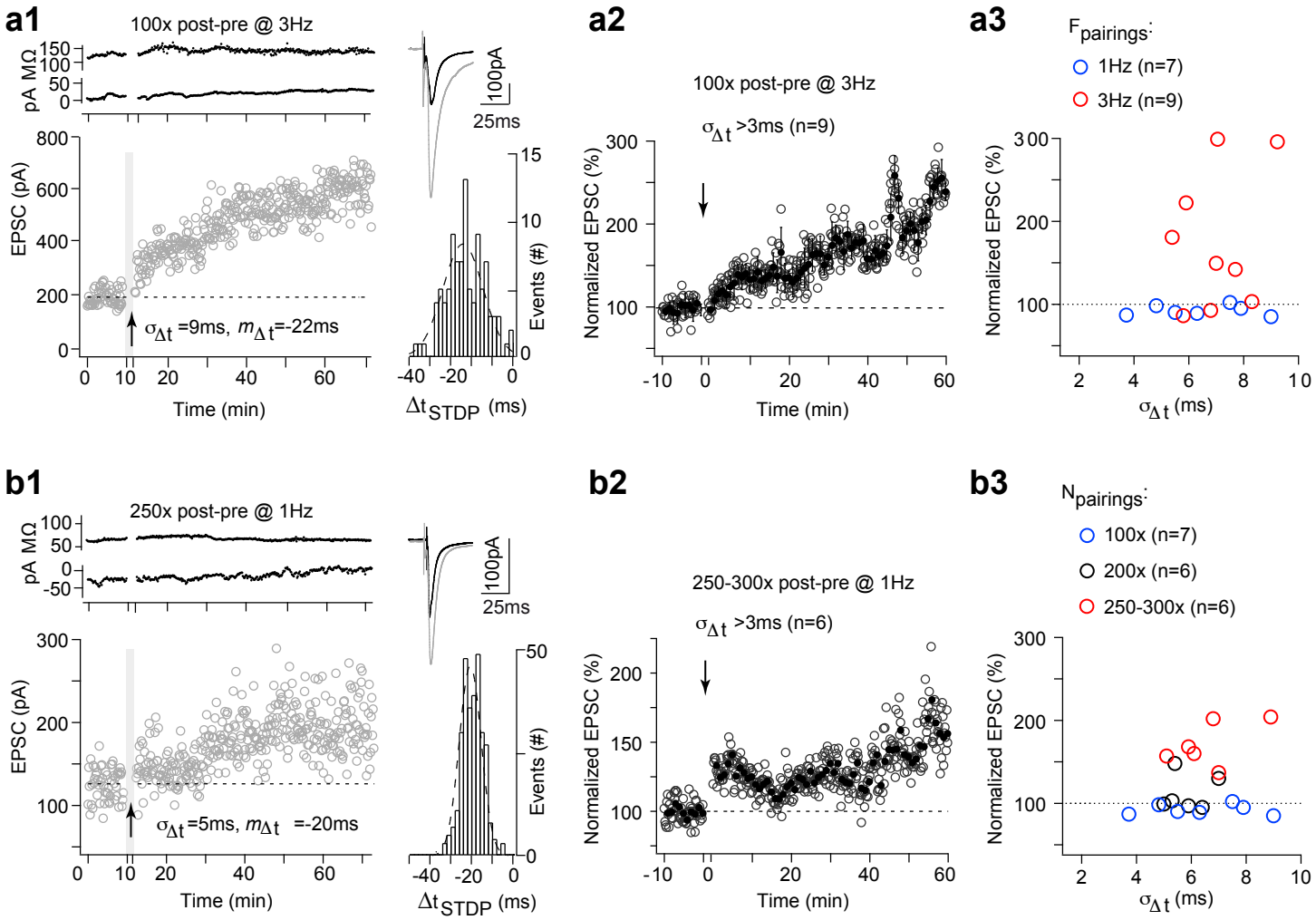
a1
100x post-pre @ 3Hz
pA MΩ
EPSC (pA)
σΔt =9ms, mΔt=-22ms
Time (min)
100pA
25ms
Events (#)
ΔtSTDP (ms)
a2
100x post-pre @ 3Hz
σΔt >3ms (n=9)
Normalized EPSC (%)
Time (min)
a3
Fpairings:
1Hz (n=7)
3Hz (n=9)
Normalized EPSC (%)
σΔt (ms)
b1
250x post-pre @ 1Hz
pA MΩ
EPSC (pA)
σΔt=5ms, mΔt =-20ms
Time (min)
100pA
25ms
Events (#)
ΔtSTDP (ms)
b2
250-300x post-pre @ 1Hz
σΔt >3ms (n=6)
Normalized EPSC (%)
Time (min)
b3
Npairings:
100x (n=7)
200x (n=6)
250-300x (n=6)
Normalized EPSC (%)
σΔt (ms)

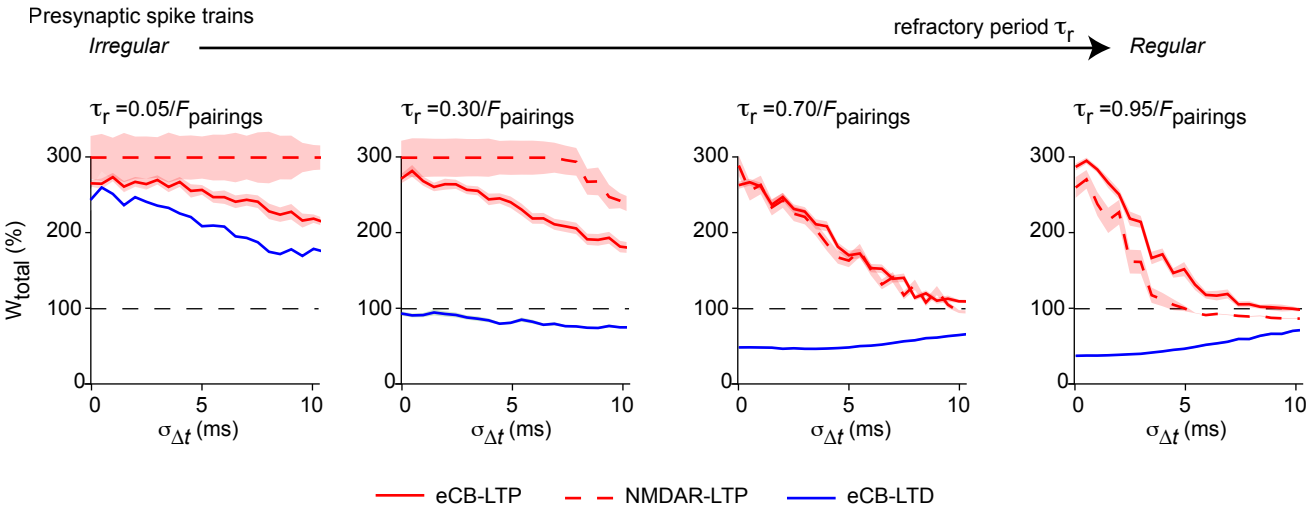
Presynaptic spike trains
Irregular
refractory period τr
Regular
τr =0.05/Fpairings
τr =0.30/Fpairings
τr =0.70/Fpairings
τr =0.95/Fpairings
Wtotal (%)
300
200
100
0
0
5
10
σΔt (ms)
eCB-LTP
NMDAR-LTP
eCB-LTD

Robustness of STDP to spike-timing jitter

Y. Cui, I. Prokin, A. Mendes, H. Berry, L. Venance

SUPPORTING INFORMATION

S1 Text - Description of the mathematical model

We describe here the mathematical model used to predict the outcome of STDP stimulations with spike timing jitter. We give here the information necessary to implement the model. Further detail and validation can be found in Cui et al (2016).

Stimulations. A STDP protocol consists in a series of N_{pairings} post- and presynaptic pairs of stimulations. We note t_{pre_i} the time at which the i^{th} presynaptic stimulation is delivered and t_{post_i} the onset time of the i^{th} postsynaptic step current stimulation, where $i = 1, \dots, N_{\text{pairings}}$. We modeled glutamate concentration in the synaptic cleft, $G(t)$, as a train of exponentially-decaying impulses triggered by presynaptic stimuli at time t_{pre_i}:

$$G(t) = G_{\max} \sum_i \exp\left(-\frac{t - t_{\text{pre}_i}}{\tau_G}\right) \Theta\left(t - t_{\text{pre}_i}\right) \quad \text{(SI1)}$$

where $G_{\max}$ is the peak glutamate concentrations and τ_G is the glutamate clearance rate. On the postsynaptic side, action currents resulting from postsynaptic stimulations were modeled according to

$$I_{\text{action}}(t) = -\text{DC}_{\max} \sum_i R\left(t, t_{\text{post}_i}, \text{DC}_{\text{dur}}\right) - \text{AP}_{\max} \sum_i \Theta\left(t - \delta - t_{\text{post}_i}\right) \exp\left(\frac{-t + \delta + t_{\text{post}_i}}{\tau_{\text{bAP}}}\right) \quad \text{(SI2)}$$

where the rectangle function $R(t, a, l) = \Theta(t - a) - \Theta(t - a - l)$, $\text{DC}_{\max}$ and DC_{dur} are the amplitude and duration of step-current injected by the patch pipette in the postsynaptic soma, $\text{AP}_{\max}$ is the amplitude of the action current producing the bAP; and τ_{bAP} is the time scale for bAP decay.

We modeled the electrical response to these stimulations in a postsynaptic element considered as a single isopotential compartment with AMPAR, NMDAR, VSCC and TRPV1 conductances

$$C_{\mathrm{m}}\frac{dV}{dt} = -g_L(V-V_{\mathrm{L}}) - I_{\mathrm{AMPAR}}(V,G(t)) - I_{\mathrm{NMDAR}}(V,G(t)) \\ -I_{\mathrm{VSCC}}(V) - I_{\mathrm{TRPV1}}(V,AEA) - I_{\mathrm{action}}(t) \quad \text{(SI3)}$$

where V is membrane potential; g_{L} and V_{L} are leak conductance and reversal potential respectively; I_{AMPAR}, I_{NMDAR}, I_{VSCC} and I_{TRPV1} are currents through AMPAR, NMDAR, L-type VSCC (v1.3) and TRPV1, respectively, and AEA stands for anandamide. NMDAR and AMPAR were modeled with two-state kinetic models and 1.0mM Mg^{2+} (Destexhe *et al.,* 1995) whereas the model and parameters for the $Ca_v1.3$ VSCC current was taken from Wolf *et al.* (2005). The TRPV1 current, including its dependence on AEA, was modeled as:

$$I_{TRPV1}(V,AEA) = g_{TRPV1}\cdot V\cdot P_{TRPV1}^{open}(V,AEA) \quad \text{(SI4)}$$

where g_{TPRV1} is the maximal conductance of TRPV1 and the mathematical expression for the P_{TRPV1}^{open} was taken from Matta and Ahern (2007).

Biochemical signaling. Free cytosolic calcium is one of the main signaling actors in the model. To model its dynamics, we assumed it can be transferred from/to two main sources: (*i*) extracellular calcium, via the plasma membrane channels of eq. (SI3) above and (*ii*) the endoplasmic reticulum (ER), via the IP3-dependent Calcium-Induced Calcium Release (CICR) system. Hence, the concentration of free cytosolic calcium C was computed according to

$$T_{\mathrm{C}}(C)\frac{dC}{dt} = J_{IP_3R} - J_{\mathrm{SERCA}} + J_{\mathrm{leak}} + J_{\mathrm{NMDAR}} + J_{\mathrm{VSCC}} + J_{\mathrm{TRPV1}} - \frac{C-C_{\mathrm{b}}}{\tau_{C_{\mathrm{b}}}} \quad \text{(SI5)}$$

where the fluxes $J_{\mathrm{IP3R}}, J_{\mathrm{SERCA}}, J_{\mathrm{leak}}$ from and to the ER in the CICR system were taken from the model of De Pittà *et al.* (2009) - see also Cui et al. (2016) and $J_{\mathrm{NMDAR}}, J_{\mathrm{VSCC}}$ and $J_{\mathrm{TRPV1}}$are the calcium fluxes from the plasma membrane channels (eq. SI3), computed as $J_{\mathrm{x}} = \xi_x \cdot I_{\mathrm{x}}$ were the ξ_x are constants, $x \in \{\mathrm{NMDAR,VSCC,TRPV1}\}$. C_{b} is the basal cytosolic calcium level resulting from equilibration with calcium diffusion out of the cell and $\tau_{C_{\mathrm{b}}}$ is the corresponding time scale. The CICR model also includes the dynamics of the fraction of inactive IP3 (inositol triphosphate) receptor channels (IP3R), h

$$\frac{\mathrm{d}h}{\mathrm{d}t} = a_2 d_2 \frac{IP3+d_1}{IP3+d_3}(1-h) - a_2 C h \quad \text{(SI6)}$$

Likewise, the dynamics of C_{ER}, the calcium concentration in the endoplasmic reticulum (ER) was given by

$$T_{C_{ER}}\left(C_{ER}\right)\frac{dC_{ER}}{dt} = -\rho_{ER}\left(J_{IP_3R} - J_{SERCA} + J_{leak}\right) \tag{SI7}$$

where ρ_{ER} is the ER to cytoplasm volume ratio. In eq.(SI5) and (SI7), T_x , $x = C$ or $C_{ER,}$ is a time scaling factor accounting for the presence of endogenous calcium buffers and expressed according to

$$T_x\left(x\right) = 1 + \frac{B_T}{K_{dB}\left(1 + x / K_{dB}\right)^2} \tag{SI8}$$

Our model also accounts for the biochemical pathways leading to the production of the endocannabinoids 2-Arachidonoylglycerol (2-AG) and AEA, and their subsequent activation of cannabinoid receptors type-1, CB_1R. Principally, the model expresses the kinetics of the following enzymatic reactions: (*i*) synthesis of DAG (diacylglycerol) and IP3 (inositol triphosphate) as a result of glutamate (G) binding of metabotropic glutamate receptors (mGluR) and subsequent activation of PLCβ as well as Ca-dependent synthesis by PLCδ, (*ii*) transformation of DAG into 2-AG by DAG Lipase α and (*iii*) synthesis of AEA by calcium-dependent fatty acid amide hydrolase (FAAH). The dynamics of this system was modeled with the following equations:

$$\frac{dIP_3}{dt} = v_\beta \frac{G}{G + K_R + K_P C/\left(C + K_\pi\right)} + \frac{v_\delta}{1 + IP_3/\kappa_d}\frac{C^2}{K_\delta^2 + C^2} - v_{3K} CaMKII * \frac{IP_3^{n_3}}{K_3^{n_3} + IP_3^{n_3}} - r_{5P} IP_3 \tag{SI9}$$

$$\frac{dDAG}{dt} = v_\beta \frac{G}{G + K_R + K_P C/\left(C + K_\pi\right)} + \frac{v_\delta}{1 + IP_3/\kappa_d}\frac{C^2}{K_\delta^2 + C^2} - \frac{r_{DGL} \cdot DAGL \cdot \varphi_{DAGL} \cdot DAG}{DAG + K_{DAGL}} - r_{DAGK} \cdot DAG \tag{SI10}$$

$$\frac{d2AG}{dt} = \frac{r_{DGL} \cdot DAGL \cdot \varphi_{DAGL} \cdot DAG}{DAG + K_{DAGL}} - r_{MAGL} 2AG \tag{SI11}$$

$$\frac{d\varphi_{DAGL}}{dt} = r_k C^{n_c}\left(1 - \varphi_{DAGL}\right) - r_p \varphi_{DAGL} \tag{SI12}$$

$$\frac{dAEA}{dt} = \upsilon_{AT} C - r_{FAAH}\frac{AEA}{K_{FAAH} + AEA} \tag{SI13}$$

where *CaMKII** is the amount of activated (phosphorylated) CaMKII (see below); φ_{DAGL} is the fraction of active DAG Lipase α and DAGL its total (activated+not activated) concentration. Eq. (SI9-SI11) account for IP3 degradation by IP3 3-kinase (3K) and inositol polyphosphate 5-phosphatase (5P), while DAG and 2AG are degraded by DAG kinase (DAGK) and monoacylglycerol lipase (MAGL), respectively.

2-AG and AEA are retrograde signaling molecules that are produced in the postsynaptic neuron but diffuse to the presynaptic cell, where they activate CB_1R. We modeled CB_1R activation by 2-AG and AEA using a simple three-state kinetic model: open (x_{CB1R}), desensitized (d_{CB1R}) and inactivated (i_{CB1R}):

$$\frac{dx_{CB1R}}{dt} = \alpha_{CB1R} \cdot eCB \cdot i_{CB1R} - \left(\beta_{CB1R} + \gamma_{CB1R}\right) x_{CB1R} \tag{SI14}$$

$$\frac{dd_{CB1R}}{dt} = -\varepsilon_{CB1R} d_{CB1R} + \gamma_{CB1R} x_{CB1R} \tag{SI15}$$

where $eCB = 2\text{-}AG + 0.10\ AEA$ and mass conservation implies $x_{\mathrm{CB1R}} + d_{\mathrm{CB1R}} + i_{\mathrm{CB1R}} = 1$. The open fraction x_{CB1R} was then used to compute CB_1R activation as

$$y_{\mathrm{CB1R}} = k_{\mathrm{CB1R}} x_{\mathrm{CB1R}} + C_1 \tag{SI16}$$

where C_1 is a constant that accounts for the modulation of presynaptic plasticity by other pathways and k_{CB1R} quantifies the strength of CB_1R activation on presynaptic plasticity.

In our model, CB_1R activation (y_{CB1R}) controls the presynaptic weight W_{pre} according to the following rule: W_{pre} decreases for intermediate values of y_{CB1R}, i.e. when y_{CB1R} is comprised between two tLTD thresholds ($\theta_{\mathrm{LTD}}^{\mathrm{start}} < y_{\mathrm{CB1R}} < \theta_{\mathrm{LTD}}^{\mathrm{stop}}$) whereas W_{pre} increases when y_{CB1R} is larger than a tLTP threshold ($y_{\mathrm{CB1R}} > \theta_{\mathrm{LTP}}^{\mathrm{start}}$). Following Cui et al. (2016), we implemented this rule as

$$\Omega(y_{\mathrm{CB1R}}) = \begin{cases} 1 - A_{\mathrm{LTD}} & \text{if } \Theta_{\mathrm{LTD}}^{\mathrm{start}} < y_{\mathrm{CB1R}} < \Theta_{\mathrm{LTD}}^{\mathrm{stop}} \\ 1 + A_{\mathrm{LTP}} & \text{if } \Theta_{\mathrm{LTP}}^{\mathrm{start}} < y_{\mathrm{CB1R}} \\ 1 & \text{otherwise} \end{cases} \tag{SI17}$$

and

$$\frac{\mathrm{d}W_{\mathrm{pre}}}{\mathrm{d}t} = \frac{\Omega(y_{\mathrm{CB1R}}) - W_{\mathrm{pre}}}{\tau_{W_{\mathrm{pre}}}(y_{\mathrm{CB1R}} + C_2)} \quad \text{(SI18)}$$

Here Ω determines the change of presynaptic plasticity, with a time scale $\tau_{W_{\mathrm{pre}}}$ set to yield rapid changes of W_{pre} for large y_{CB1R}values and very slow changes at very low y_{CB1R}:

$$\tau_{W_{\mathrm{pre}}}(\mathrm{x}) = \frac{P_1}{P_2^{P_3} + x^{P_3}} + P_4 \quad \text{(SI19)}$$

To account for experimental observation that the presynaptic weight ranges from about 50 to 300%, W_{pre} was clipped to 3.0 (hard bound).

Postsynaptic plasticity in the model was based on the activation by calcium of calmodulin and CaMKII and the regulation of this system by PKA, calcineurin and protein phosphatase 1 (PP1). The model of Cui et al (2016) for this subsection is based on the model proposed in Graupner & Brunel (2007). In this model the concentration of the calcium/calmodulin complex with four calcium ions bound (CaM) is considered at equilibrium and computed as:

$$CaM = \frac{CaMT}{1 + \sum_{i=1}^{4}(C^i \cdot \prod_{j=5-i}^{4} K_j)} \quad \text{(SI20)}$$

where *CaMT* is the total calmodulin concentration and K_i stands for the equilibrium constant of the binding of the i^{th} calcium ion to calmodulin. Each CaMKII enzyme consists of two subunits, each of which contains 6 phosphorylation sites, thus defining 14 phosphorylation states per subunit. Denoting y_i, i=0…13 the concentrations of subunit in phosphorylation state i, the model of Graupner & Burnel (2007) expresses their dynamics as:

$$
\begin{aligned}
\frac{dy_1}{dt} &= 6k_6\gamma^2 y_0 - (4k_6\gamma^2 + k_7\gamma + k_{10})y_1 + 2k_{10}\sigma_2^4 \\
\frac{dy_2}{dt} &= (k_7\gamma + k_6\gamma^2)y_1 - (3k_6\gamma^2 + k_7\gamma + 2k_{10})y_2 + k_{10}(y_5 + \sigma_5^7) \\
\frac{dy_3}{dt} &= 2k_6\gamma^2 y_1 - 2(k_7\gamma + k_6\gamma^2 + k_{10})y_3 + k_{10}(\sigma_5^7 + 3y_8) \\
\frac{dy_4}{dt} &= k_6\gamma^2 y_1 - 2(k_7\gamma + k_6\gamma^2 + k_{10})y_4 + k_{10}(y_6 + y_7) \\
\frac{dy_5}{dt} &= k_7\gamma(\sigma_2^3 - y_5) + k_6\gamma^2(y_2 - 2y_5) + k_{10}(2y_9 + y_{10} - 3y_5) \\
\frac{dy_6}{dt} &= k_6\gamma^2(\sigma_2^3 - y_6) + k_7\gamma(2y_4 - 2y_6) + k_{10}(-3y_6 + \sigma_9^{11} + y_{11}) \\
\frac{dy_7}{dt} &= k_6\gamma^2(y_2 + 2y_4 - y_7) + k_7\gamma(y_3 - 2y_7) + k_{10}(-3y_7 + \sigma_9^{11} + y_{11}) \\
\frac{dy_8}{dt} &= k_6\gamma^2 y_3 - 3k_7\gamma y_8 + k_{10}(y_{10} - 3y_8) \\
\frac{dy_9}{dt} &= k_7\gamma(\sigma_5^7 - y_9) + k_6\gamma^2(y_5 - y_9) + k_{10}(-4y_9 + 2y_{12}) \\
\frac{dy_{10}}{dt} &= k_6\gamma^2 y_5 + k_6\gamma^2 y_6 + k_7\gamma(y_7 + 3y_8 - 2y_{10}) + k_{10}(2y_{12} - 4y_{10}) \\
\frac{dy_{11}}{dt} &= k_7\gamma(y_6 - 2y_{11}) + k_6\gamma^2 y_7 + k_{10}(y_{12} - 4y_{11}) \\
\frac{dy_{12}}{dt} &= k_6\gamma^2 y_9 + k_7\gamma(2\sigma_9^{11} - y_9 - y_{12}) + k_{10}(6y_{13} - 5y_{12}) \\
\frac{dy_{13}}{dt} &= k_7\gamma y_{12} - 6k_{10}y_{13}
\end{aligned}
\qquad \text{(SI21)}
$$

where $\sigma_i^j = \sum_{k=i}^{j} y_k$ and mass conservation implies $y_0 = 2CaMKII_0 - \sigma_1^{13}$, where $CaMKII_0$ is the total CaMKII concentration. In eq. (SI21) above the probabilities that CaM binds to phosphorylated (γ) and dephosphorylated (γ^*) subunit of CaMKII are computed as $\gamma = CaM/(CaM + K_5)$ and $\gamma^* = CaM/(CaM + K_9)$. Moreover, the rate of subunit dephosphorylation (k_{10}) is given by $k_{10} = k_{12}PP1/(K_M + CaMKII^*)$ where K_M is a constant, $PP1$ is the concentration of PP1. $CaMKII^*$ is the total concentration of phosphorylated subunits of CaMKII computed accross all possible states of phosphorylation $CaMKII^* = \sum_{i=0}^{13} m_i y_i$ where m_i is the number of the phosphorylated subunits of CaMKII in state i and y_i.

Finally, the model of Graupner & Brunel (2007) assumes that, in addition to calcineurin (CaN), PKA activity depends on CaM according to a Hill-function activation:

$$
\nu_x(CaM) = k_x^0 + \frac{k_x}{1 + (K_x/CaM)^{n_x}} \qquad \text{(SI22)}
$$

where $x = CaN$ or PKA, The interaction between PP1 and I1 is then described as:

$$
\begin{aligned}
\frac{dI1}{dt} &= \frac{dPP1}{dt} - \nu_{CaN} I1 + \nu_{PKA} I1_0 \\
\frac{dPP1}{dt} &= -k_{13} I1 \cdot PP1 + k_{-13}(PP1_0 - PP1)
\end{aligned}
\qquad \text{(SI23)}
$$

where $PP1_0$ and $I1_0$ are total PP1 and I1 concentrations, respectively.

In agreement with Cui et al. (2016) and Graupner & Brunel (2007), we assumed that postsynaptic plasticity is directly proportional to the calcium-dependent activation of CaMKII and set:

$$W_{\text{post}} = 1 + 3.5\frac{CaMKII^*}{CaMKII^*_{\text{max}}} \quad \text{(SI24)}$$

where $CaMKII^*_{\text{max}}$ is the maximal concentration of activate (phosphorylated).

Finally, the total synaptic weight was taken as the product of the presynaptic and the postsynaptic contributions above:

$$W_{\text{total}} = W_{\text{pre}}W_{\text{post}} \quad \text{(SI25)}$$

Model implementation and numerics. Our mathematical model comprises 36 ordinary differential equations and close to 150 parameters, among which more than one half is constrained by experimental data. Initial conditions were set to the steady-state of each variable in the absence of stimulation. Numerical solution was obtained with the LSODA solver from the ODEPACK fortran77 library with absolute and relative tolerances both equal to 10^{-7}. Initial conditions were set to the steady-state of each variable in the absence of stimulation. Numerical integration proceeded until the synaptic weights reach stable values (typically observed around t ≈ 5min after the stimulation protocol). We used the final values of the pre- and postsynaptic weights to compute the total synaptic weight change due to the stimulations. Importantly, with the exception of the stimulation protocols, *we have used the exact same equations and parameter values as in* Cui et al. (2016). The list of parameters and their estimated values is given in S2 Table. The current study employs stochastic simulations since the stimulation protocol is stochastic (while the rest of the model is deterministic). Therefore, the model was calibrated using experimental data from deterministic stimulation

protocols (Cui et al., 2016) and we tested here whether it can make successful predictions when we applied stochastic stimulation protocols, for which the model was not calibrated. The results are thus averages over N_{trials} realizations. N_{trials} was varied from 30 to 500 depending on the smoothness of the averaged curves and values of SEM, but N_{trials}=50 in most of the simulations. The computer code of the model is available online from https://github.com/iprokin/Cx-Str-STDP and https://senselab.med.yale.edu/modeldb/ShowModel.cshtml?model=187605.

S2 Table – Parameter values

A. Intracellular dynamics

Description	Name	Values	Units	Reference
I_{NMDAR} to Ca flow conversion	ξ_{NMDAR}	98	µM/pCol	set to match Ca2+ amplitudes in [1]
I_{VSCC} to Ca flow conversion	ξ_{VSCC}	140	µM/pCol	set to match Ca2+ amplitudes in [2]
I_{TRPV1} to Ca flow conversion	ξ_{TRPV1}	290	µM/pCol	set to match Ca2+ amplitudes in [1]
Total endogenous Ca buffer	B_T	4.5	µM	Estimated from our experimental data
Basal cytoplasmic [Ca]	C_b	0.1	µM	[1,3]
Time scale for Ca exit	τ_{Cb}	0.007	s	Idem
Endogenous Ca buffer affinity	K_{dB}	0.5	µM	[3,4]
ER-to-cytosol volume ratio	ρ_{ER}	0.3	-	Adapted from [4]
IP3R binding rate (inactivation)	a_2	0.5	µM/s	Idem
Maximal SERCA pump rate	v_{ER}	8	µM/s	Idem
IP3R affinity for IP3	d_3	0.9434	µM	[5]
Maximal IP3R rate	r_C	4	1/s	Adapted from [5]
Basal [Ca] in the ER	$Ca_{ER,b}$	65	µM	[6]
Ca leak from the ER	r_l	0.1	1/s	[5]
IP3R affinity for Ca	d_5	0.12	µM	Adapted from [5]
IP3R dissociation constant	d_2	3.049	µM	Idem
SERCA pump affinity for Ca	K_{ER}	0.05	µM	[5]
IP3R affinity for IP3	d_1	0.13	µM	Idem
PLCδ product inhibition	κ_d	1.5	µM	Idem
PLCδ Ca-activation	K_δ	0.1	µM	Idem
5P-IP maximal rate	r_{5P}	0.2	1/s	Adapted from [5]
PI3K maximal rate	v_{3K}	0.001	µM/s	Idem
PI3K Ca-activation constant	K_D	1.5	µM	Idem
PLCδ maximal rate	v_δ	0.02	µM/s	[5]
PI3K affinity for IP3	K_3	1	µM	Idem
Glutamate affinity to mGluR	K_R	1.3	µM	Idem
regulation by PLCβ termination	K_P	10	µM	Idem
PLCβ maximal rate	v_β	0.8	µM/s	Adapted from [5]
PKC Ca-activation constant	K_π	0.6	µM	[5]
Total CaMKIIα concentration	$CaMKII_0$	16.6	µM	[7]
Total Calmodulin concentration	$CaMT$	0.07085	µM	Adapted from [7]
PKA Hill number	n_{PKA}	3	-	Idem

Referenced articles: [1] Sabatini, B.L., Oertner, T.O. and Svoboda, K. (2002) *Neuron* 33(3):439-452 [2] Carter, A.G. and Sabatini, B.L. (2004) *Neuron* 44(3):483-493 [3] Jackson, M.B. and Redman, S.J. (2003) *J Neurosci* 23:1612–1621 [4] Nägerl, U.V. *et al.* (2000) *Biophys J* 79: 3009–3018 [5] De Pittà M. *et al.* (2009) *J Biol Phys* 35:383-411 [6] Solovyova, N. *et al.* (2002) *EMBO J* 21:622-630 [7] Graupner, M. and Brunel, N. (2007) *PLoS Comput Biol* 3:e221.

B. Electrophysiology

Description	Name	Values	Units	Reference
TRPV1R max. conductance	g_{TRPV1}	0.0003	nS	Estimated from our experimental data
Permeability of L-type VSCC	p_{VSCC}	0.00000102	µM/s	Value of [1], scaled to ~5,000 spines, radius 1 µm
AMPAR maximal conductance	g_{AMPAR}	5.1	nS	Estimated from our experimental data
AMPAR closing rate constant	β_{AMPAR}	190	1/s	Adapted from [2]
AMPAR opening rate constant	α_{AMPAR}	1.02	1/(µM.s)	Idem
NMDAR maximal conductance	g_{NMDAR}	1.53	nS	Estimated from our experimental data
Magnesium concentration	Mg	1	mM	Directly measured in our experiments
NMDAR opening rate constant	α_{NMDAR}	0.072	1/(µM.s)	Set to emulate the experimental kinetics of NMDAR-transported Ca in [3]
NMDAR closing rate constant	β_{NMDAR}	100	1/s	Idem
Resting membrane potential	V_L	-70	mV	Directly measured in our experiments
Leak conductance	g_L	10	nS	Idem
Membrane capacitance	C_m	0.1	nF	Idem
Extracellular Ca2+ concentration	Ca_{out}	5000	µM	[1]
Duration of depolarization step	DC_{dur}	0.03	s	From the experimental stimulation protocol
Amplitude of depolarization step	$DC_{\max}$	495	pA	Idem
Amplitude of action current	$AP_{\max}$	7020	pA	[4]
Time constant of action current	τ_{bAP}	0.001	s	Idem
Glutamate peak concentration in the cleft	$G_{\max}$	2000	µM	Estimated from our experimental data
Glutamate decay time constant in the cleft	τ_G	0.005	s	Estimated from our experimental data
Delay to bAP outset	δ	0.015	s	From the experimental stimulation protocol
Stimulation frequency	F_{pairings}	1	Hz	From the experimental stimulation protocol

Referenced articles: [1] Wolf, J.A. *et al.* (2005) *J Neurosci* 25(40):9080-9095 [2] Destexhe, A., Mainen, Z., and Sejnowski, T. (1994) *J Comput Neurosci* 1:195-230 [3] Sabatini, B.L., Oertner, T.O. and Svoboda, K. (2002) *Neuron* 33(3):439-452 [4] Fino, E., *et al*. (2010) *J Physiol* 588:3045-3062.

C. Endocannabinoid dynamics

Description	Name	Values	Units	Reference
Scaling factor for endocannabinoid contribution to plasticity	k_{CB1R}	3000	1/µM	Estimated from our experimental data
presynaptic plasticity time scale	P_1	1e-9	s	Set to yield rapid / slow changes of Wpre for high / low 2-AG values, respectively
presynaptic plasticity time scale	P_2	1e-5	-	Idem
presynaptic plasticity time scale	P_3	7	-	Idem
presynaptic plasticity time scale	P_4	2	s	Idem
The lower limit of LTD induction	θ_{LTD}^{start}	0.027	-	Estimated from our experimental data
The upper limit of LTD induction	θ_{LTD}^{stop}	0.047	-	Idem
The constant determining the rate of LTD induction	A_{LTD}	0.65	-	Idem
The lower limit of LTP induction	θ_{LTP}^{start}	0.087	-	Idem
The constant determining the rate of LTP induction	A_{LTP}	10.8	-	Idem
CB1R opening rate constant	α_{CB1R}	0.2402	1/(µM.s)	Idem
CB1R closing rate constant	β_{CB1R}	11.072	1/s	Idem
CB1R desensitization rate constant	γ_{CB1R}	416.38	1/s	Idem
CB1R closing rate constant	ε_{CB1R}	0.047796	1/s	Idem
DAGL α affinity for DAG	K_{DAGL}	30	µM	[1]
Maximal rate of MAG lipase	r_{MAGL}	0.5	µM/s	Set for rapid turnover dynamics.
Maximal DAGL α rate	r_{DGL}	20000	µM/s	Idem
DAG kinase rate	r_{DAGK}	2	s^{-1}	Idem
Hill number for DAGL activation by Ca	n_c	6	-	Estimated from our experimental data
DAGL dephosphorylation rate	r_P	380	s^{-1}	Idem
DAGL phosphorylation rate	r_K	50	$\mu M^{-1}.s^{-1}$	Idem
Total DAGL concentration	$DAGL$	1	µM	Idem
N-acetyltransferase activity	v_{AT}	0.2	1/s	Idem
FAAH Michaelis-Menten constant	K_{FAAH}	1	µM	[1]
FAAH enzyme activity	r_{FAAH}	4	µM/s	Estimated from our experimental data

Referenced articles: [1] Okamoto, Y. et *al.* (2004) *J Biol Chem* 279:5298-5305.

S3 Text – Mechanisms of STDP expression in the model

We give here an overview of the mechanisms that give rise to the expression of eCB-tLTP, eCB-tLTD and NMDAR-tLTP in our mathematical model. All the examples given here concern regular (deterministic) STDP protocols with constant IPI and spike timings.

Our model combines the two signaling pathways involved in cortico-striatal STDP: a first signaling pathway leading from NMDAR to calmodulin and CaMKII with a second that couples mGluR and cytosolic calcium to eCB production and the resulting activation of CB_1R (see Fig. 1f1). In the model, we assume that the total synaptic weight (W_{Total}) is the product of presynaptic (W_{Pre}) and postsynaptic (W_{Post}) weights (see Supporting Information S1).

On the postsynaptic side, W_{Post} is proportional to the amount of CaMKII activated by the NMDAR pathway. CaMKII in our model forms a bistable system that settles at long times either on a "DOWN" state where CaMKII is mostly inactive (no plasticity) or on an "UP" state characterized by high levels of activated CaMKII (Fig. 2b1) (NMDAR-tLTP). In the example of the figure, the time needed for CaMKII dephosphorylation is larger than the interval between two successive pairings, so activated CaMKII accumulates with the number of pairings during the protocol. For a transition from the UP to the DOWN state to occur, the amount of activated CaMKII needs to overcome the separatrix between the two states. The separatrix is reached in the example of *Supplementary Figure S2* (in Supporting Information S4 below) for circa 50-60 post-pre pairings (with Δt_{STDP} =-15 ms) (Fig. S2a1). Therefore, in the conditions of Figure S2 (short post-pre pairings), W_{Post} converges to the UP state (potentiation) only when the STDP protocol comprises > 50 post-pre pairings. With pre-post pairings, the calcium released after each pairing activates less calmodulin than with post-pre protocols. As a result, activated CaMKII never reaches the threshold for the UP state (Fig. S2a2). To summarize, the model successfully reproduces the experimental observations that (*i*) NMDAR-dependent tLTP emerges after 50-75 short post-pre pairings and (*ii*) no NMDAR-dependent LTP is obtained with pre-post pairings (Cui et al., 2016).

When a stimulation protocol composed of 100 pairings is applied, the evolution of the amplitude of the triggered calcium peaks is biphasic (Fig. S2c): it increases up to 10-20 pairings and decreases afterwards to settle to constant amplitude after circa 50 pairings. For the first 10-20 stimulations, the iterated activation of mGluRs leads to the accumulation of IP3, which contributes an extra influx of calcium from the endoplasmic reticulum through calcium-induced calcium release. This extra-boost of cytoplasmic calcium however vanishes when the number of pairings increases further because the concentration of calcium in the ER

decreases. This decay ER calcium eventually compensates the effect of IP3 accumulation on the calcium-induced calcium release, thus stabilizing the amplitude of the calcium peaks for $N_{pairings}$>50. Moreover, since the width of the postsynaptic calcium peak in the model is larger with post-pre than pre-post pairings (Fig S2b), the fraction of calcium-activated DAGLα is much larger for post-pre pairings. As a result, the amplitude of eCB peaks and, ultimately, the amplitude of the fraction of activated CB_1R (y_{CB1R}), show a more pronounced biphasic profile (Fig S2d). The biphasic trend is further amplified at the level of CB_1R activation because of CB_1R receptor desensitization that amplifies the decay above 20 pairings (Fig S2d). The amplitude of the y_{CB1R} peaks increases sharply for the first 10-20 pairings, and progressively decays afterwards to converge to constant amplitude. As show in the figure, y_{CB1R} reaches large values only for short post-pre pairings (Δt_{STDP} around -15 ms) while even short pre-post pairings ($0< \Delta t_{STDP} <10$ ms) do not give rise to such large amplitude peaks.

The dynamics of the level of y_{CB1R} is responsible for the emergence of eCB-dependent plasticity in the model. Indeed, in the model, W_{Pre} depends on y_{CB1R} with the piecewise constant function shown in Figure S2e and its 3 thresholds Θ_{LTD}^{start}, Θ_{LTD}^{stop} and Θ_{LTP}^{start}: if y_{CB1R} reaches moderate amounts, i.e. lies within $[\Theta_{LTD}^{start}, \Theta_{LTD}^{stop}]$, W_{Pre} decays (thus emulating eCB-tLTD); whereas W_{Pre} increases (eCB-tLTP) if $y_{CB1R} > \Theta_{LTP}^{start}$ (see the dashed lines in Fig. S2d and summary in Fig. S2e). With short pre-post pairings ($10 < \Delta t_{STDP} <40$ ms), y_{CB1R} enters the LTD range during most of protocol so each pairing contributes a increment of W_{Pre} reduction. Since W_{Post} is not changed with positive, pre-post pairings (Fig. S2a2), pre-post pairings globally lead to a progressive reduction of W_{Total}, i.e. the expression of eCB-tLTP. The situation is different for post-pre pairings. The amplitude of y_{CB1R} peaks overcomes Θ_{LTP}^{start} for ≈ 5 to 30 post-pre-pairings with short Δt_{STDP} (around -15 ms), yielding a strong increase of W_{Pre}. Given that more that 50 post-pre pairings are needed to alter W_{Post} (Fig. S2a1), the expansion of W_{Pre} leads to eCB-tLTP. However, when $N_{pairings} > 30$ post-pre pairings, y_{CB1R} amplitude gets back below Θ_{LTP}^{start} so that the initial increase of W_{Pre} does not continue beyond 30 post-pre pairings. This property of the model dynamics emulated the experimental observation that eCB-tLTP disappears when the number of pairings becomes larger than 25-30.

Therefore, the mechanisms that lead to the expression of eCB-dependent plasticity with regular deterministic stimulation protocols in our model can be summarized as follow. eCB-tLTD requires moderate levels of CB_1R activation that are reached with pre-post but not pre-post pairings. The expression of eCB-tLTP however demands larger amounts of CB_1R

activation, which are reached only during the first 5-30 post-pre pairings, where every component of the system contributes maximally to CB_1R activation. When the number of post-pre pairings becomes larger than 30, calcium efflux from the internal calcium stores decreases and CB_1R desensitization increases: CB_1R activation becomes insufficient to support such high values of CB_1R activation, so eCB-tLTP vanishes.

S4 Figure – Supplementary Figures

Figure S1

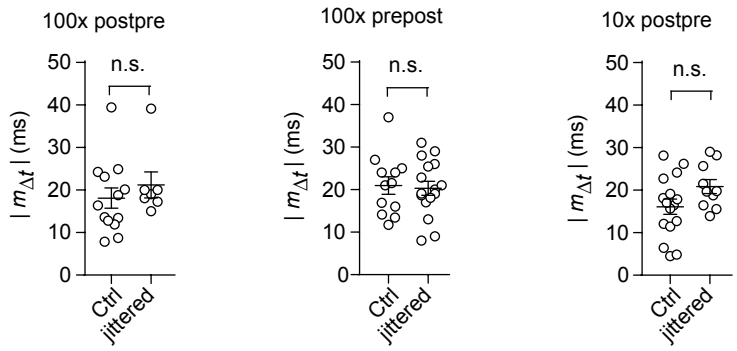

Supplementary Figure 1: $m_{\Delta t}$ values were not significantly different among STDP paradigms. $m_{\Delta t}$ were not significantly different in control and jittered conditions for 100 post-pre, 100 pre-post and 10 post-pre pairings (empty circles: individual neurons; black circle: average). Error bars represent the SEM. ns: not significant.

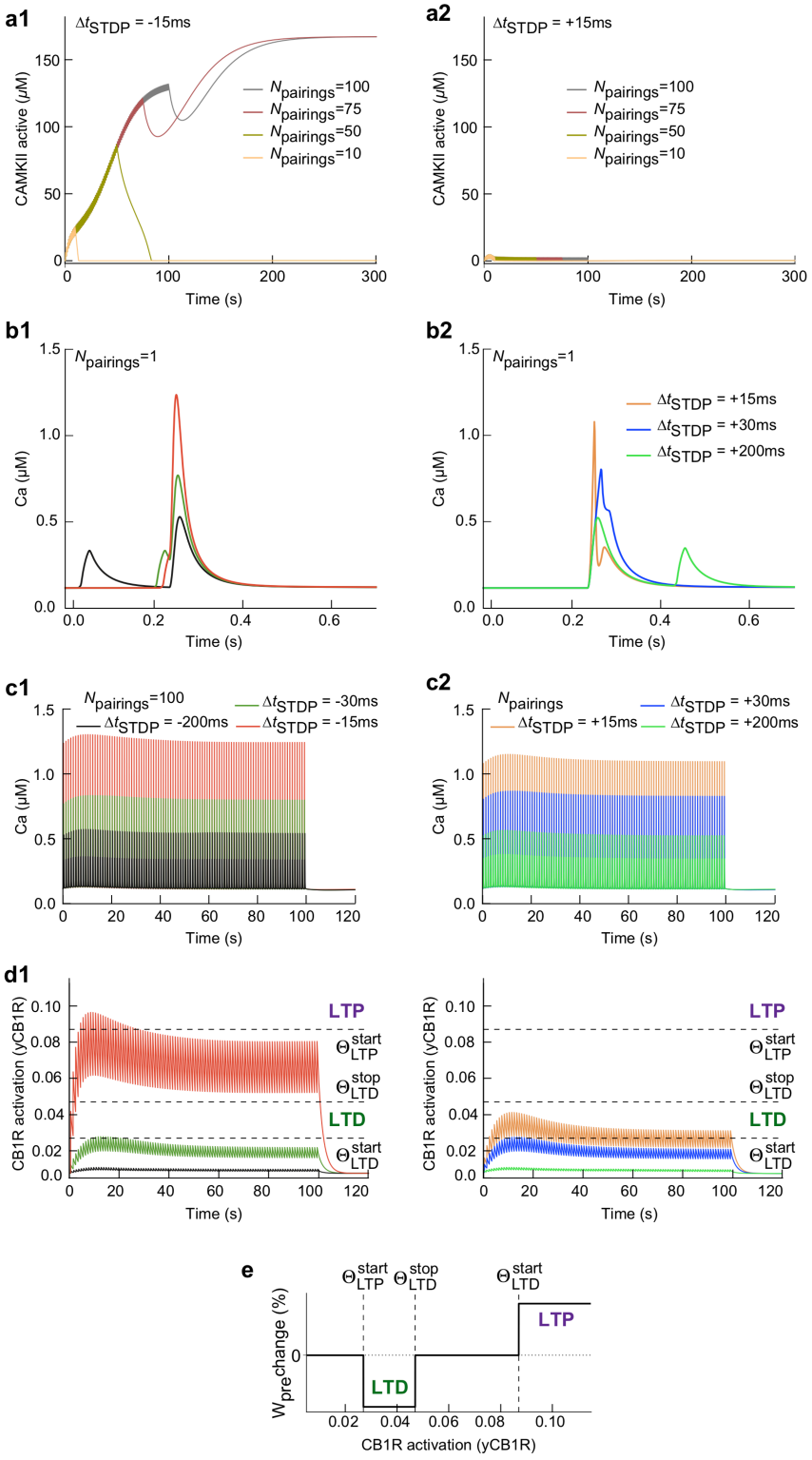

Supplementary Figure 2: **Mechanisms of STDP expression in the model with deterministic stimulation protocols**.

(**a**) Changes in the amount of active CaMKII starting from the down (non-activated) state. The number of pairings, N_{pairings}, is indicated for spike-timing Δt_{STDP} = -15 (**a1**) or + 15 (**a2**) ms. (**b**) Intracellular calcium changes for the first pairing in post-pre (**b1**) or pre-post (**b2**) pairing protocols. (**c**) Predicted dynamics of the cytoplasmic calcium for 100 post-pre (**c1**) or 100 pre-post pairings (**c2**) and corresponding activation of CB1R, y_{CB1R} (**d**). The spike-timing Δt_{STDP} for each curve is indicated in the legend. (**e**) The presynaptic weight W_{Pre} changes as a function of y_{CB1R}: it decreases (LTD) when y_{CB1R} reaches intermediate values and it increases (LTP) if y_{CB1R} overcomes the LTP threshold. The corresponding thresholds are reported in D as dashed lines. For all the simulations shown, the stimulation protocols were deterministic (regular) with a frequency of 1Hz.

SUPPLEMENTARY REFERENCES

Cui Y, Prokin I, Xu H, Delord B, Genet S, Venance L, Berry H. (2016) Endocannabinoid dynamics gate spike-timing dependent depression and potentiation. eLife **5**:1–32.

De Pittà M, Goldberg M, Volman V, Berry H, Ben-Jacob E. (2009) Glutamate regulation of calcium and IP3 oscillating and pulsating dynamics in astrocytes. J Biol Phys **35**:383–411.

Destexhe A, Mainen ZF, Sejnowski TJ (1995) Fast kinetic models for simulating AMPA, NMDA, GABA a and GABA B receptors. The Neurobiology of Computation:9–14.

Graupner M, Brunel N (2007) STDP in a bistable synapse model based on CaMKII and associated signaling pathways. PLoS Comput Biol **3**:e221.

Matta JA, Ahern GP (2007) Voltage is a partial activator of rat thermosensitive TRP channels. J Physiol **585**:469–482.

Wolf JA, Moyer JT, Lazarewicz MT, Contreras D, Benoit-Marand M, O'Donnell P, Finkel LH (2005) NMDA/AMPA ratio impacts state transitions and entrainment to oscillations in a computational model of the nucleus accumbens medium spiny projection neuron. J Neurosci **25**:9080–9095.